CHAPTER 5   UNCERTAINTY ANALYSIS

5.1   UA for Forces and Moment and Motions

The purpose is to develop an uncertainty analysis (UA) procedure for planar motion mechanism (PMM) tests measurements including forces and moment and motions. The approach follows errors/uncertainties definitions, systematic/random categorizations, and large sample size/normal distribution 95% level of confidence assumptions, as provided by the AIAA (1999), ANSI/ASME (1998), and AGARD (1994) standard and guidelines. The present UA procedure is for a model scale towing tank PMM test for an un-appended model ship except bilge keels (i.e. without shafts, struts, propellers, and rudders) which is mounted free to heave and pitch, but fixed in roll. Bias and precision limits and total uncertainties for multiple runs are estimated for the non-dimensional forces and moment and motions in model scale for four types of PMM tests (static drift, pure yaw, pure sway, and yaw and drift). Other PMM tests, such as static rudder, static drift and rudder, static drift and heel, dynamic yaw and rudder, dynamic yaw and drift and rudder, are not considered. This procedure does not provide UA for hydrodynamic derivatives derived from the forces and moment data or their effect on the full scale maneuvering simulations.

Limitations of present UA procedures are listed as follows: The effect of data conditioning such as filtering or fairing, for example, Fourier Series (FS) reconstructions for the measured forces /moment and motions is not counted in this UA procedure. This procedure assumes that the measured forces/moment is the sum of those from all forces/moment gauges used for the case of multiple gauge system, and that the inertia forces/moment from parts for model installation are subtracted from the total measured forces and moments if the parts are suspended from the loadcells. This procedure also assumes that the model ship is free to heave and pitch, and fixed in roll. The effect of deviations from the upright position such as roll or heel angle is not considered in this

procedure. Finally, carriage speed is assumed to be constant, so the effect of acceleration caused by fluctuating carriage speed during runs is not considered.

Present UA procedure is developed in an international collaboration between the IIHR-Hydroscience & Engineering (IIHR, USA), Force Technology (FORCE, Denmark), Instituto Nazionale per Studi ed Esperienze di Architettura Navale (INSEAN, Italy), and the $24^{th} - 25^{th}$ International Towing Tank Conference (ITTC) Maneuvering Committee (MC). The collaboration includes overlapping tests using the same model geometry for comparisons of the results and for identifications of possible facility biases and scale effects. The basis of the UA procedure was first developed by FORCE (Simonsen 2004), followed by an application to INSEAN (Benedetti et al. 2006), and extended herein by including the definitions of the asymmetry bias and the facility bias as presented at the following sections.

The procedure has been accepted by the 25th ITTC (2008) as an ITTC Recommended Procedure and Guidelines (7.5-02-06.04 Uncertainty Analysis: Forces and moment; Example for Planar Motion Mechanism Test). For which the proposed procedure was reviewed by the Specialist Committee on Uncertainty Analysis (SCUA) of the 25th ITTC. The review included comments on ten (10) topics: 1) Jitter Method, 2) Assumptions, 3) Model Length, 4) Drift Angle, 5) Mass Uncertainty, 6) Force, 7) Calibration and Acquisition, 8) Water Density and Temperature, 9) Precision limit, and 10) Carriage speed. The comments focus on the traceability of error estimations to the known uncertainty such as NIST (National Institute of Standards and Technology) standards and as well on suggestions of alternative approaches that seem to follow more closely the ISO GUM (1995) and/or the US Guide (1997). In general, the comments can be grouped into three categories: (A) comments which lead to constructive improvements in the proposed procedure; (B) comments regarding insufficient descriptions in the proposed procedure; and (C) conceptual differences between AIAA/ASME and ISO/US Guide UA approaches. Topics 1), 3), 5), and 6) are considered as type (A) which are helpful for improving

the proposed procedure. Topics 2), 4) and 8) are considered as type (B) for which descriptions in the proposed procedure are insufficient and need to be revised based on the comments. Lastly, topics 7), 9), and 10) are considered as type (C) which may arise from differences between AIAA/ASME and ISO/US Guide UA approaches. Accordingly, herein the UA procedure was corrected for and/or added supplementary descriptions as per most of the editorial and technical comments, except for type (C) comments for which the proposed procedures based on the AIAA/ASME were retained. In general, differences between the AIAA/ASME and ISO/US Guide UA are usually conceptual and the final UA results do not differ significantly (Coleman and Steel, 1999). Nonetheless, as a new version of UA standard, the ASME PTC 19.1-2005 (2005) was released by the ASME, where more of harmonization between the two approaches was made, the type (C) comments can also be achieved for the next revision of the present PMM UA procedures by following the new ASME standards.

The organization is as follows: Definitions and estimation procedures for bias and precision limits and total uncertainty are provided in sections 5.1.1, 5.1.2, and 5.1.3, respectively, and UA results are discussed in section 5.1.4. A conceptual, data asymmetry bias is defined and evaluated in sections 5.1.5. Next, the UA results from three facilities data are compared in Section 5.1.6. Another conceptual, facility bias is defined and evaluated in Section 5.1.7.

5.1.1 Bias limits

For the forces and moment data, X, Y, and N, the DRE's (3.7) and (3.8) for the dynamic tests and static drift test, respectively, can be rewritten in functional forms as

$$r(x) = r(L, T, x_G, y_G, m, I_z, \rho, u, v, r, \dot{u}, \dot{v}, \dot{r}, F) \tag{5.1}$$

and

$$r(x) = r(L, T, \rho, U_C, F) \tag{5.2}$$

respectively, where the result r can be X, Y, or N, and the symbol F represents the forces and moment F_x, F_y, or M_z, respectively. For the motion data, the DRE (3.9) for z is re-written in a functional form as

$$z(x) = z(z_{mm}, L) \tag{5.3}$$

However, DRE's are not used for θ and ϕ data. From the DRE's (5.1) and (5.2), the error propagation equations can be written as

$$B_r^2 = \theta_L^2 B_L^2 + \theta_T^2 B_T^2 + \theta_{x_G}^2 B_{x_G}^2 + \theta_{y_G}^2 B_{y_G}^2 + \theta_m^2 B_m^2 + \theta_{I_z}^2 B_{I_z}^2 + \theta_\rho^2 B_\rho^2 +$$

$$\theta_u^2 B_u^2 + \theta_v^2 B_v^2 + \theta_r^2 B_r^2 + \theta_{\dot{u}}^2 B_{\dot{u}}^2 + \theta_{\dot{v}}^2 B_{\dot{v}}^2 + \theta_{\dot{r}}^2 B_{\dot{r}}^2 + \theta_F^2 B_F^2 \tag{5.4}$$

and

$$B_r^2 = \theta_L^2 B_L^2 + \theta_T^2 B_T^2 + \theta_\rho^2 B_\rho^2 + \theta_{U_C}^2 B_{U_C}^2 + \theta_F^2 B_F^2 \tag{5.5}$$

for dynamic tests and static drift test, respectively. Of the element biases in (5.4), the bias limits for motion parameters, B_u, B_v, B_r, $B_{\dot{u}}$, $B_{\dot{v}}$, and $B_{\dot{r}}$, are through their own error propagation equations from the DRE's (5.2) as:

$$B_u^2 = \theta_{U_C}^2 B_{U_C}^2 + \theta_\psi^2 B_\psi^2 + \theta_{v_{PMM}}^2 B_{v_{PMM}}^2 \tag{5.6a}$$

$$B_v^2 = \theta_{U_C}^2 B_{U_C}^2 + \theta_\psi^2 B_\psi^2 + \theta_{v_{PMM}}^2 B_{v_{PMM}}^2 \tag{5.6b}$$

$$B_r^2 = B_{r_{PMM}}^2 \tag{5.6c}$$

$$B_{\dot{u}}^2 = \theta_{U_C}^2 B_{U_C}^2 + \theta_\psi^2 B_\psi^2 + \theta_r^2 B_r^2 + \theta_{v_{PMM}}^2 B_{v_{PMM}}^2 + \theta_{\dot{v}_{PMM}}^2 B_{\dot{v}_{PMM}}^2 \tag{5.6d}$$

$$B_{\dot{v}}^2 = \theta_{U_C}^2 B_{U_C}^2 + \theta_\psi^2 B_\psi^2 + \theta_r^2 B_r^2 + \theta_{v_{PMM}}^2 B_{v_{PMM}}^2 + \theta_{\dot{v}_{PMM}}^2 B_{\dot{v}_{PMM}}^2 \tag{5.6e}$$

$$B_{\dot{r}}^2 = B_{\dot{r}_{PMM}}^2 \tag{5.6f}$$

Further element biases, $B_{v_{PMM}}$, $B_{\dot{v}_{PMM}}$, B_ψ, $B_{r_{PMM}}$, $B_{\dot{r}_{PMM}}$ in (5.6) are again through their own DRE's in (3.1) as:

$$B_{v_{PMM}}^2 = \theta_N^2 B_N^2 + \theta_{S_{mm}}^2 B_{S_{mm}}^2 + \theta_t^2 B_t^2 \tag{5.7a}$$

$$B_{\dot{v}_{PMM}}^2 = \theta_N^2 B_N^2 + \theta_{S_{mm}}^2 B_{S_{mm}}^2 + \theta_t^2 B_t^2 \tag{5.7b}$$

$$B_\psi^2 = \theta_{\psi_{max}}^2 B_{\psi_{max}}^2 + \theta_N^2 B_N^2 + \theta_t^2 B_t^2 + \theta_\beta^2 B_\beta^2 \tag{5.7c}$$

$$B_{r_{PMM}}^2 = \theta_{\psi_{max}}^2 B_{\psi_{max}}^2 + \theta_N^2 B_N^2 + \theta_t^2 B_t^2 \tag{5.7d}$$

$$B_{\dot{r}_{PMM}}^2 = \theta_{\psi_{max}}^2 B_{\psi_{max}}^2 + \theta_N^2 B_N^2 + \theta_t^2 B_t^2 \tag{5.7e}$$

Thus, the biases of the motion parameters are from five elemental biases, $B_{S_{mm}}$, B_N, B_t, B_β, and $B_{\psi_{max}}$, through (5.7) and then (5.6) with B_{U_C}. Next for the motion data, the error propagation equations are written as

$$B_z^2 = \theta_{z_{mm}}^2 B_{z_{mm}}^2 + \theta_L^2 B_L^2 \tag{5.8a}$$

$$B_\theta = B_\theta \tag{5.8b}$$

$$B_\phi = B_\phi \tag{5.8c}$$

The sensitivity coefficients, θ's, in (5.4) – (5.8) are evaluated analytically by differentiating the DRE's with respect to each variable of interest, x, such that

$$\theta_x = \frac{\partial r}{\partial x} \tag{5.9}$$

where r is the DRE variable. For a reference, the θ's for (5.4) and (5.5) are summarized in Tables 5-1 and 5-2 for dynamic and static tests, respectively. Note that the sensitivity coefficients can also be evaluated numerically by using, for example, a 'Jitter method' (Moffat 1982 and Coleman and Steele 1999). The estimations of the fifteen element bias limits, B_L, B_T, B_{x_G}, B_{y_G}, B_m, B_{I_z}, B_ρ, B_{U_C}, B_u, B_v, B_r, $B_{\dot{u}}$, $B_{\dot{v}}$, $B_{\dot{r}}$, and B_F, are as per Si-

mon et al. (2004), and the estimations of biases for the motion data, $B_{z_{mm}}$, B_θ, and B_ϕ are also presented.

   Global variables (L, T, x_G, y_G, m, I_z, ρ): B_L is from the model manufacturing accuracy ± 1 mm in all coordinates. Model 5512 was manufactured at NSWC (Naval Surface Warfare Center) of US Navy and underwent a laser-scan for the exterior surface geometry. Result confirmed the manufacturing accuracy. B_T is the RSS of two uncorrelated element biases, $B_{T,1}$ and $B_{T,2}$. $B_{T,1}$ is from the precisions of the draft-markers on the model surface, estimated at 0.1 mm, and $B_{T,2}$ is from the model ballasting accuracy with respect to the draft markers, 1 mm, from a tape measurement. B_{x_G} is the RSS of two uncorrelated element biases, $B_{x_G,1}$ and $B_{x_G,2}$. $B_{x_G,1}$ is the deviation of actual model center of gravity (COG) from its designed position, 5 mm, from empirical estimations based on model manufacturing. $B_{x_G,2}$ is the model installation error, estimated at 2 mm based on the installation accuracies. B_{y_G} is the RSS of two elemental biases, $B_{y_G,1} = 2$ mm and $B_{y_G,2} = 1$ mm, similarly as per B_{x_G}. B_m is the RSS of individual mass component measurement error B_{m_i} such that $B_m^2 = \sum_i B_{m_i}^2$. The element mass components (See Section 3.2) are measured with two types of commercial strain-gauge type scales. These are a Virtual Measurement & Control Inc. VW-321-S-30 Bench Scale and a Masterline MLG-500 Hanging Crane Scale, with 30 Kg and 227 Kg of maximum capacities, respectively, and with 0.023 Kg and 0.045 Kg reading accuracies, respectively. B_{I_z} is from the separate measurements of I_z. B_ρ is from the ITTC 1963 density-temperature formula for fresh water, $\rho(T) = 999.784 + 0.0638T - 0.00865T^2 + 0.0000631T^3$. The error propagation equation for ρ can be written as $B_\rho^2 = (\partial\rho/\partial T)^2 B_T^2$ where B_T is the errors in water temperature T reading. Water temperature is measured with a resistive-type probe and signal conditioner, at a water-depth corresponding to model mid-draft. The temperature sensor and probe is an Omega Engineering Inc. DP465 model, specified with the probe accuracy as $B_T = \pm 0.2°C$. The uncertainties in the density formula were assumed as negligible.

Carriage speed: B_{U_C} is evaluated end-to-end by calibrating U_C with respect to the reference speed, $U_{\text{ref}} = \Delta L / \Delta t$. The reference speed is achieved by measuring the travel-time Δt for a known distance ΔL. Then, B_{U_C} is defined as

$$B_{U_C}^2 = B_{U_C,\text{ref}}^2 + B_{U_C,\text{fit}}^2 \qquad (5.10)$$

where the $B_{U_C,\text{ref}}$ is from the accuracy of U_{ref} and the $B_{U_C,\text{fit}}$ is from scatter in the U_C calibration data set in relation to a linear least-squares regression curve fit. $B_{U_C,\text{ref}}$ is by applying the error propagation equation to U_{ref} such that

$$B_{U_C,\text{ref}}^2 = \theta_{\Delta L}^2 B_{\Delta L}^2 + \theta_{\Delta t}^2 B_{\Delta t}^2 \qquad (5.11)$$

where $\theta_{\Delta L} = \partial U_{\text{ref}} / \partial \Delta L$ and $\theta_{\Delta t} = \partial U_{\text{ref}} / \partial \Delta t$, and $B_{\Delta L} = 0.005$ m from the errors in tape measure of ΔL and $B_{\Delta t} = 0.0001$ sec from the U_C sampling time interval 0.001 sec. $B_{U_C,\text{fit}}$ is evaluated as $2 \times SEE$ where the standard estimate of error (SEE) is from Coleman and Steele (1999) as,

$$B_{U_C,\text{fit}} = 2 \cdot SEE = 2 \cdot \sum_{i=1}^{M} \sqrt{\frac{(Y_i - Y_i')^2}{M-2}} \qquad (5.12)$$

where Y_i is the measured U_C during the calibration, Y_i' is from the regression equation, and M is the number of data in the calibration. Calibration was done for three U_{ref}'s, 0.754, 1.531, and 2.241 m/s, with three repeat tests. Results revealed that $B_{U_C,\text{fit}}$ (0.010 m/s) is predominant over $B_{U_C,\text{ref}}$ (0.0014 m/s).

  <u>Motion parameters</u>: B_u, B_v, B_r, $B_{\dot{u}}$, $B_{\dot{v}}$, $B_{\dot{r}}$ are from elemental biases, $B_{S_{mm}}$, B_N, B_t, B_β, $B_{\psi_{max}}$ and B_{U_C} through the error propagation equations (5.7) and (5.6). B_{U_C} is as per above. $B_{S_{mm}}$ is from the sway crank amplitude setting uncertainty, 0.5 mm. B_N is the uncertainty in PMM motion frequency, 0.0006 rpm, and B_t is the uncertainty in data-

sampling timescale, 0.001 sec, both determined empirically. B_β is the RSS of two uncorrelated elemental errors such that

$$B_\beta^2 = B_{\beta,\text{align}}^2 + B_{\beta,\text{drift}}^2 \tag{5.13}$$

where $B_{\beta,\text{align}}$ is from the errors in the initial model-installation with respect to straight towing direction and $B_{\beta,\text{drift}}$ is from the errors in setting the model at designated drift angles. The model alignment procedure consists of two steps, first the alignment of the strong-back with respect to towing direction and then alignment of the model ship with respect to the strong-back centerline. For the first step, the strong-back is aligned to the carriage towing direction guided by a laser-beam with its source fixed at the towing tank ceiling. For this, first the laser-beam is adjusted to point to the forward-end-center-point (C_fwd) of strong-back, and the carriage is driven forward until the laser-beam hits the rear-end of strong-back. Then, the distance between the rear-end-center-point (C_rear) of strong-back and the laser-beam, d, is measured, and then the orientation of strong-back is adjusted to compensate approximately a half d. The procedure is repeated until d becomes fairly smaller than the laser-beam diameter. For the second step, two plumb-bob strings are hanging from the C_fwd and C_rear, and the model center-line is aligned with the plumb-bob strings within a tolerance, ϵ. By assuming the two procedures are uncorrelated,

$$B_{\beta,align}^2 = \left(\arctan\frac{d}{D}\right)^2 + \left(\arctan\frac{\epsilon}{D}\right)^2 \tag{5.14}$$

where D is the distance between C_fwd and C_rear, i.e. the strong-back length. $B_{\beta,\text{align}}$ was evaluated as 0.03° for $d = 2$ mm corresponding to the laser-beam diameter, $\epsilon = 1$mm, and $D = 4$ m. Next, $B_{\beta,\text{drift}}$ is attained end-to-end by calibrating the β readings with respect to reference angles. The reference drift angle β_ref is achieved by measuring the travel-distance, C, of a fixed-point at the model while it is rotated from straight-heading to a

designated β angle position, and measuring the distance, R, between the point and the rotation pivot (See Fig. 5-1), such that $\beta_{\text{ref}} = \arccos(1 - C^2/2R^2)$. Subsequently, $B_{\beta,\text{drift}}$ is defined as the RSS of $B_{\beta,\text{drift,ref}}$ and $B_{\beta,\text{drift,fit}}$ similarly as B_{U_C} in (5.10),

$$B_{\beta,\text{drift}}^2 = B_{\beta,\text{drift,ref}}^2 + B_{\beta,\text{drift,fit}}^2 \tag{5.15}$$

$B_{\beta,\text{drift,ref}}$ is the uncertainty in β_{ref} defined as $B_{\beta,\text{drift,ref}}^2 = \theta_C^2 B_C^2 + \theta_R^2 B_R^2$, where $\theta_C = \partial\beta_{\text{ref}}/\partial C$ and $\theta_R = \partial\beta_{\text{ref}}/\partial R$ and B_C and B_R are the biases in C and R measurements. $B_{\beta,\text{drift,fit}} = 2 \cdot SEE$, similarly as per (5.12) for $Y = \beta$ and $Y' = \beta_{\text{ref}}$. From a calibration for twelve β_{ref} values (M = 12) between $\pm 12°$, $B_{\beta,\text{drift}}$ was evaluated as $0.22°$ as per (5.15) and with $B_C = B_R = 1$ mm. Lastly, $B_{\psi\,\text{max}}$ is the same as $B_{\beta,\text{drift}}$.

Forces and moment: B_F is from uncertainties in 1) force/moment gauges calibration, 2) model motions from the pre-described PMM motions, and 3) data-sampling time-scales. The uncertainties 1) is common for dynamic and static test data and is composed of two element biases $B_{F,\text{ref}}$ and $B_{F,\text{fit}}$. The uncertainties 2) differ for dynamic and static test; $B_{F,u}$, $B_{F,\dot{u}}$, $B_{F,v}$, $B_{F,\dot{v}}$, $B_{F,r}$, and $B_{F,\dot{r}}$ for the former and $B_{F,\beta}$ and $B_{F,\text{align}}$ for the latter. The uncertainty 3) is only for dynamic test data, $B_{F,t}$. Accordingly, B_F is the RSS of those element biases as

$$B_F^2 = B_{F,\text{ref}}^2 + B_{F,\text{fit}}^2 + B_{F,u}^2 + B_{F,\dot{u}}^2 + B_{F,v}^2 + B_{F,\dot{v}}^2 + B_{F,r}^2 + B_{F,\dot{r}}^2 + B_{F,t}^2 \tag{5.16}$$

for dynamic tests and

$$B_F^2 = B_{F,\text{ref}}^2 + B_{F,\text{fit}}^2 + B_{F,\text{align}}^2 + B_{F,\beta}^2 \tag{5.17}$$

for static drift test, respectively.

$B_{F,\text{ref}}$ is the uncertainty in the reference force or moment, F_{ref}, for gauges calibrations, i.e., the accuracy of calibration standard weights W. In that, $F_{\text{ref}} = W$ for force-

gauge calibrations, and $F_{\text{ref}} = W \times L$ for moment-gauge calibrations, respectively, where L is the moment-arm. When calibrations are repeated for several W's, then $B_{F,\text{ref}}$ is the RSS of the individual standard weight uncertainty B_{W_i} such that

$$B_{F,\text{ref}}^2 = \Sigma_i B_{W_i}^2 \qquad (5.18)$$

for $F = F_x$ and $F = F_y$, and

$$B_{F,\text{ref}}^2 = \Sigma_i \left(\theta_{W_i}^2 B_{W_i}^2 + \theta_L^2 B_L^2 \right) \qquad (5.19)$$

for $F = M_z$, where W_i is the individual standard weight, $\theta_{W_i} = \partial F_{\text{ref}} / \partial W_i$ and $\theta_L = \partial F_{\text{ref}} / \partial L$ as per (5.9) for $\chi = F_{\text{ref}}$, and B_{W_i} and B_L are the errors in the standard weight and the moment arm dimension, respectively. Calibration was done with ASTM Class 4 standard weights with a 0.002% tolerance, from which $B_{F,\text{ref}}$ was rated at 0.002% of the full-scale for F_x and F_y gauges (50 N), and 0.014% for M_z gauge (200 Nm).

$B_{F,\text{fit}}$ is from the scatter in the calibration data set in relation to a linear least-squares regression curve fit, i.e., the volt-to-force conversion error of the force/moment gauges. In general, $B_{F,\text{fit}}$ exhibits dependency on the magnitude of F applied, rather than a fixed-amount such as $2 \cdot SEE$, and is fitted to a linear function of F as

$$B_{F,\text{fit}} = a|F| + b \qquad (5.20)$$

For this, the differences between the measured and applied forces, i.e., $\Delta F = \left| F - F_{\text{ref}} \right|$, during the calibration are linear-curve-fitted as $\Delta F_{95\%} = a|F_{\text{ref}}| + b$ to evaluate the coefficients a and b in (5.20). The $\Delta F_{95\%}$ is defined as

$$\Delta F_{95\%} = \overline{\Delta F} + P_{\overline{\Delta F}} \qquad (5.21)$$

where $\overline{\Delta F}$ is the mean ΔF from the M repeat measurements for each W_i and $P_{\overline{\Delta F}}$ is the precision limit of the ΔF measurements as per (5.26) for $r = \Delta F$ shown in the following

Section 5.1.2. Statistically, for M $\geq$ 10, the true ΔF falls within $\pm \Delta F_{95\%}$ in 95 out of 100 cases. Calibrations were repeated twelve times for each W_i (M = 12), and $B_{F,\text{fit}}$ was rated at 0.3%, 0.4%, and 0.3% of full-scales of the F_x, F_y, and M_z gauges, respectively. For the calibration, the g value of 9.8031 m/s^2 based on the local latitude of Iowa City, Iowa, USA (Halliday & Resnick 1981) was used and the local buoyancy was assumed as negligible.

$B_{F,\text{align}}$ and $B_{F,\beta}$ for static drift test data are the biases of F from $B_{\beta,\text{align}}$ in (5.14) and $B_{\beta,\text{drift}}$ in (5.15), respectively, defined as

$$B_{F,\text{align}}^2 = \theta_\beta^2 B_{\beta,\text{align}}^2 \tag{5.22}$$

$$B_{F,\beta}^2 = \theta_\beta^2 B_{\beta,\text{drift}}^2 \tag{5.23}$$

where the sensitivities $\theta_\beta = \partial F / \partial \beta$ was evaluated by curve-fitting the static drift F data as polynomial functions of β.

$B_{F,u}$, $B_{F,v}$, $B_{F,r}$, $B_{F,\dot{u}}$, $B_{F,\dot{v}}$, and $B_{F,\dot{r}}$ are the errors in F due to the uncertainties in the motion parameters, B_u, B_v, B_r, $B_{\dot{u}}$, $B_{\dot{v}}$, and $B_{\dot{r}}$, respectively, and are defined as

$$B_{F,x}^2 = \theta_x^2 B_x^2 \tag{5.24}$$

for $x = u, v, r, \dot{u}, \dot{v}, \dot{r}, t$, respectively, where $\theta_x = \partial F / \partial x$ and B_x's are the same as (5.6). Without the DRE for F, derivatives $\partial F / \partial x$'s are approximated by modeling the measured forces and moment F time-histories as polynomial functions of motion parameters, $\tilde{F}$, such that $\partial F / \partial x \approx \partial \tilde{F} / \partial x$. The model functions $\tilde{F}$ for each dynamic test are summarized in Table 5-3, where the coefficients, A's, B's, and C's of $\tilde{F}$ are determined by applying a least-squares-error method for multiple variables. For the implementation, a singular-value-decomposition (SVD) method was used solving the least-square matrix, and several coefficients such as A_r, A_{rr}, $A_{\dot{u}}$, B_r, $B_{\dot{u}}$, $B_{\dot{r}}$, C_r, $C_{\dot{u}}$, and $C_{\dot{r}}$ for the pure sway $\tilde{F}$ are set to zero to avoid singular matrices.

$B_{F,t}$ is the error due to uncertainties of the data sampling time scale B_t, written as

$$B_{F,t}^2 = \theta_t^2 B_t^2 \tag{5.25}$$

where $\theta_t = \partial F / \partial t$ was evaluated by differentiating numerically the time-histories of F, and B_t is the uncertainties in the data-sampling timescale.

Motion data: Of the four element biases in (8) for the motion data, B_L is the same as presented above and $B_{z_{mm}}$, B_θ, and B_ϕ are from the measurement errors of the Krypton motion tracker. As per the Krypton camera verification report, a value of ± 0.1 mm is used for $B_{z_{mm}}$ since the target is in zone #1 of the camera module field of view (See Section 3.7.2). Biases for pitch and roll data B_θ and B_ϕ, respectively, are 0.04° for both from the previous UA results (Irvine et al. 2008).

5.1.2   Precision limits

The precision limits are determined from 12 repeat tests. The datasets are spaced in time at least 12 minutes between tests to minimize flow disturbances from previous runs, while spanning over a time period, usually one day, that is large relative to time scales of the factors that influence variability of the measurements. The same model ship, PMM motion generator, loadcell, and motion tracker are used for repeat tests due to limitations of time and experiment resources. The model is not dismounted and re-installed during the repeat tests. However, the PMM motion control parameters, such as drift angle, sway crank amplitude, or maximum heading angle settings are changed between tests. The precision limits are computed with the standard multiple-test equation

$$P_r = \frac{t S_{\bar{r}}}{\sqrt{M}} \tag{5.26}$$

for $r = X, Y, N, z, \theta$, and ϕ, where $t = 2$ is the coverage factor for 95% confidence level and $M = 12$ is the number of repeat tests. $S_{\bar{r}}$ is the standard deviation defined as

$$S_{\bar{r}} = \left[\sum_{k=1}^{M} \frac{(r_k - \bar{r})}{M-1} \right]^{\frac{1}{2}} \tag{5.27}$$

and

$$\bar{r} = \frac{1}{M} \sum_{k=1}^{M} r_k \tag{5.28}$$

where, r_k is X, Y, N, z, θ, or ϕ of the kth run.

5.1.3 Total Uncertainty limits

The total uncertainty for the average result is the RSS of B_r and P_r.

$$U_r^2 = B_r^2 + P_r^2 \tag{5.29}$$

A conceptual asymmetry bias B_{asym} is defined if data asymmetry with respect to the xz-plane is larger than U_r estimations, as following:

$$U_{T_1}^2 = U_r^2 + B_{asym}^2 \tag{5.30}$$

Another conceptual facility bias B_{FB} is defined if the difference of each facility data from the facility mean is larger than U_{T_1}, as following:

$$U_{T_2}^2 = U_{T_1}^2 + B_{FB}^2 \tag{5.31}$$

Definitions, estimation procedures, and estimation results of the B_{asym} and B_{FB} are provided in sections 5.1.5 and 5.1.7, respectively.

5.1.4 UA Results and Discussions

UA results for the elemental biases $B_{L_{PP}}$, B_{T_m}, B_{x_G}, B_{y_G}, B_m, B_{I_z}, B_ρ, B_{U_C}, B_u, B_v, B_r, $B_{\dot{u}}$, $B_{\dot{v}}$, $B_{\dot{r}}$, and B_F in (5.4) and (5.5) are presented first with identifications of the primary error sources, and then, the total bias B_r and precision P_r limits and their contri-

butions to total uncertainty U_r are presented. For the dynamic test data, the period-mean values of uncertainty limits, $\langle B \rangle$, $\langle P \rangle$, and $\langle U \rangle$, are defined as

$$\langle B, P, U \rangle = \frac{1}{T} \int_0^T (B, P, U) dt \tag{5.32}$$

where T is the PMM motion period. Note for static drift and pure yaw data that, presented herein are the average values for three Fr cases otherwise mentioned, and also for static drift data that, the $\langle B \rangle$, $\langle P \rangle$, and $\langle U \rangle$ values are the same as B, P, and U values, respectively. Typically, the uncertainty limits B, P, and U are presented in %D values, where D is defined in different ways according to the characteristics of the variable and/or according to specific type of the test. For anti-symmetry variables (v, $\dot{v}$, r, $\dot{r}$, v_{PMM}, $\dot{v}_{PMM}$, ψ, r_{PMM}, $\dot{r}_{PMM}$, F_y, M_z, Y, N, and ϕ), D is defined as the dynamic range of the variable, and for symmetry variables (u, F_x, X, z, and θ), D is the period-mean value of the variable with defined similarly as (5.32).

Global variables and carriage speed: $B_{L_{PP}}$, B_{T_m}, B_{x_G}, B_{y_G}, B_m, B_{I_z}, B_ρ, and B_{U_C} are presented in Table 5-4 and compared with their nominal values (D). Typically, B values are fairly smaller than D. $B_{L_{PP}}$ is 0.07% of L_{PP}. B_{T_m} is 0.7% of T_m. B_{x_G} is 31.3% of x_G. $B_{y_G} = 2$ mm. B_m is 0.1% of m for both of the free- and fixed-model cases. B_{I_z} is about 4% of I_z for both the free- and fixed-model cases. B_ρ is negligibly small 0.004% of ρ at T = 20°C. B_{U_C} is 1.4%, 0.7%, and 0.5% of U_C for Fr = 0.138, 0.280, and 0.410, respectively.

Motion parameters: $B_{v_{PMM}}$, $B_{\dot{v}_{PMM}}$, B_ψ, $B_{r_{PMM}}$, and $B_{\dot{r}_{PMM}}$ are presented in Table 5-5 for pure sway, pure yaw, and yaw and drift tests at $Fr = 0.280$, where at the top part of the table $B_{S_{mm}}$, B_N, B_t, B_β, and $B_{\psi_{max}}$ are also summarized. In general, $\langle B_{v_{PMM}} \rangle$, $\langle B_{\dot{v}_{PMM}} \rangle$, $\langle B_\psi \rangle$, $\langle B_{r_{PMM}} \rangle$, and $\langle B_{\dot{r}_{PMM}} \rangle$ values are all less than 1% of their own D values except for a few cases where D values are negligibly small. $B_{v_{PMM}}$ and $B_{\dot{v}_{PMM}}$ are mostly

from $B_{S_{mm}}$, about 93%. B_ψ is from both B_β and $B_{\psi_{max}}$, about 67% and 33%, respective-ly. $B_{r_{PMM}}$ and $B_{\dot{r}_{PMM}}$ are from $B_{\psi_{max}}$, almost 100%.

B_u, B_v, B_r, $B_{\dot{u}}$, $B_{\dot{v}}$, and $B_{\dot{r}}$ are presented at the lower part of Table 5-5. $\langle B_u \rangle$ is 0.7% for all test types, and mostly (99%) contributed from B_{U_C}. $\langle B_v \rangle$ is about 2% except for PY where D value is negligibly small, and mostly (96%) contributed from B_ψ that is from B_β and $B_{\psi_{max}}$. $\langle B_r \rangle$ is 0.7% except for PS where D value is negligibly small, and is the same as $\langle B_{r_{PMM}} \rangle$ that is from $B_{\psi_{max}}$. $\langle B_{\dot{u}} \rangle$ is about 1% except for pure sway where again D is negligible, and mainly contributed from B_{U_C}, B_ψ, and $B_{r_{PMM}}$ for pure sway, pure yaw, and yaw and drift, respectively, 63%, 84%, and 87%, respectively, which are again from B_β and $B_{\psi_{max}}$. $\langle B_{\dot{v}} \rangle$ is about 4% and mainly contributed from B_{U_C} and $B_{\dot{v}_{PMM}}$ where the latter is from $B_{S_{mm}}$. $\langle B_{\dot{r}} \rangle$ is 0.7% except for PS for which D is negligible, and is the same as $\langle B_{\dot{r}_{PMM}} \rangle$ that is from $B_{\psi_{max}}$.

Forces and moment: B_F's are presented in Table 5-6 including contributions of the element biases. For static drift, B_F is about 1%, 3%, and 3%, in averages for three Fr cases for F_x, F_y, and M_z, respectively, and mainly contributed from $B_{F,\beta}$, 76%, 97%, and 96%, respectively. For dynamic test, $\langle B_F \rangle$ values are about 1% in general and the main contributors are different by the test type and by the variable. For pure sway, $B_{F,v}$ is the primary bias contributing about 95%. For pure yaw, $B_{F,r}$ is the common primary bias for F_x, F_y, and M_z, contributing 17%, 96%, and 67%, respectively, and $B_{F,\text{fit}}$ and $B_{F,\dot{v}}$ are al-so main biases for F_x, contributing 32% and 34%, and $B_{F,\dot{r}}$ for M_z, contributing 34%, in averages for three Fr cases. For yaw and drift, $B_{F,u}$ is the primary bias for F_x and $B_{F,v}$ is for F_y and M_z, contributing about 57%, and $B_{F,r}$ is the common primary bias contributing about 31%.

Total Bias Limits B_r's are summarized in Table 5-7 including the contributions of individual element biases. In general, the primary biases vary by the variable and by the test type. For static drift, B_{U_C} and B_F are the common primary biases for X, Y, and N da-ta, where B_T is also large for X. For pure sway, the primary bias is B_u for X and B_F for Y

and N, respectively. For pure yaw, B_u is the primary bias for X, B_F is the primary and B_r is the secondary bias and for Y, and B_F is the primary and B_u is the secondary bias and B_{I_z} is also large for N. For yaw and drift, B_u is the primary and B_F is the secondary bias for X, and B_F is the primary and B_u is the secondary bias for both Y and N, and B_{I_z} is also large for N. The primary biases for static drift and pure yaw data exhibit Fr trends. For static drift, the contribution of B_{U_C} decreases with Fr, whereas B_T and B_F show the opposite trend. For pure yaw, in general, the trend varies by the variable: the contribution of B_u decreases with Fr for X; the contribution of B_r is almost constant with Fr, whereas that of B_F increases with Fr for Y; the contribution of B_u is decreasing and that of B_F is increasing with Fr for N, respectively.

The sources of the primary biases and their propagations were traced back through Tables 5-7, 5-6, and 5-5 and then 5-4, summarized in Table 5-8. For static drift, B_{U_C} and B_F are the common primary biases for B_X, B_Y, and B_N, where the former is directly from U_C and the latter is from β propagated through $B_{F,\beta}$. For dynamic tests, B_u is the primary bias of B_X, commonly for pure sway, pure yaw, and yaw and drift tests, and is propagated from U_C through B_{U_C}. On the other hand, B_F is the primary bias for both B_Y and B_N, but from different sources propagated through different paths; from β and ψ_{max} for pure sway through B_ψ, B_v, and then $B_{F,v}$, from ψ_{max} for pure yaw through $B_{r_{PMM}}$, B_r, and then $B_{F,r}$, and from β and ψ_{max} for yaw and drift test through $B_\psi / B_{r_{PMM}}$, B_v / B_r, and then $B_{F,v} / B_{F,r}$, respectively. Consequently, U_C is the primary bias source for X and β and ψ_{max} are for Y and N, suggesting that improvement of carriage speed (U_C) control is important for X and precise angle-setting for β and $\psi_{\max}$ is important for Y and N to reduce the bias errors.

The overall UA results are summarized in Table 5-9 including the total bias B_r and precision P_r limits and their contributions to the total uncertainty U_r. Herein, $\langle B_r \rangle$, $\langle P_r \rangle$, and $\langle U_r \rangle$ values (B_r, P_r, and U_r values for static drift) are presented in % D, in the order of X, Y, and N, and in averages for three Fr cases for static drift and pure yaw. In

general, uncertainties are larger for dynamic test data than static drift data, and larger for X data than Y and N. For static drift, B_r is predominant, contributing to U_r about 87%, 93%, 91%, respectively, and P_r is relatively small, contributing to U_r about 13%, 8%, 9%, respectively, indicating most DRE variable results are highly repeatable. U_r is about 2%, 4%, 3%, respectively, reasonably small but comparatively larger than resistance test uncertainty $U_{CT} = 1\%$ of C_T (Longo et al. 2005). Additional error sources for static drift, such as B_β, may explain the higher uncertainty level than the resistance test result. For dynamic tests, in general $\langle B_r \rangle$ is dominant for Y and N, contributing to $\langle U_r \rangle$ about: 63% and 94% for pure sway; 67% and 89% for pure yaw; and 80% and 92% for yaw and drift, whereas $\langle P_r \rangle$ is dominant for X, contributing to $\langle U_r \rangle$ about 75% for pure sway, 70% for pure yaw, and 71% for yaw and drift. $\langle U_r \rangle$ is about: 5%, 2%, 2%, respectively, for pure sway, similar with static drift; 8%, 5%, 1%, respectively, for pure yaw, usually larger than static drift and pure sway, and tends to decrease with Fr in general; and 7%, 4%, 2%, respectively, larger than static drift and pure sway but similar with pure yaw.

The UA results for motion data z and θ are also presented in Table 5-9. For z, $\langle U_r \rangle$ is about 6%, 5%, 8%, and 3% for static drift, pure sway, pure yaw, and yaw and drift, where usually $\langle P_r \rangle$ is predominant over 80% for all tests. For θ, $\langle U_r \rangle$ is about 81%, 28%, 29%, and 15%, respectively, where $\langle B_r \rangle$ is predominant over 80% in general.

5.1.5   Asymmetry Bias

Static drift test X, Y, N, z and θ are presented in Fig. 5-2 for both positive and negative β ranges. Contrary to expectations, test results show large asymmetry of data between positive and negative β. The asymmetry of X is more apparent and seemingly larger than the U_r limits estimated with (5.29) shown at $\beta = -10°$. Similar asymmetry is observed from the motion data, although seemingly better symmetry. With the drift angle bias $B_{F,\beta}$ and the model ship alignment bias $B_{F,align}$ accounted previously in the UA procedures in Section 3.1, further errors such as model fabrication error and/or initial

heeling of the model, probably from imperfect weight ballasting, maybe possible reasons for the asymmetry.

In order to quantify the asymmetry of data $r = X, Y, N, z$, and θ, data asymmetry Δr_{asym} is defined as

$$\Delta_{asym} = |r^+ - r^-|/r_m \qquad (5.33)$$

where r^+ is the value at positive β, r^- is at negative β with proper sign changes for anti-symmetric variables such as Y and N, and r_m is the average of r^+ and r^-. At Fr = 0.280, Δ_{asym} is about 20% for X at $\beta = 10°$, which is significantly larger than the total uncertainty width $2U_r = 4.3\%$ of r_m, and Δ_{asym} increases up to 40 % at $\beta = 20°$. Whereas Δ_{asym} for Y and N exhibit an opposite trend; decreasing with β, and within the $2U_r$ at β = 10°. Due to the lack of solid explanations for those data asymmetry, the mean value r_m is taken as the representing data, and the amount of data asymmetry is added to the total uncertainty U_r defined as a conceptual bias B_{asym} as

$$B_{asym}^2 = D_{asym}^2 - U_r^2 \qquad (5.34)$$

if $D_{asym} > U_r$, whereas B_{asym} equals zero if $D_{asym} \leq U_r$. Here, D_{asym} is the difference between r and r_m such that

$$D_{asym} = |r - r_m| \qquad (5.35)$$

Subsequently, the total uncertainty U_{T_1} is defined as per equation (30).

Defining asymmetry of dynamic test data, however, may not be as straightforward as for static drift test data. Nonetheless, the use of symmetry and anti-symmetry charac-teristics of the dynamic test variables can be a possible approach. The time-histories of the dynamic test data are shown in Figure 5-3 for pure sway, pure yaw, and yaw and drift tests, respectively. For pure sway data, as an example, the odd-order harmonics of the symmetric variables such as X, z, and θ and the even-order harmonics of the anti-

symmetric variables such as Y and N are not expected from their Fourier-Series (FS) expansions since the pure sway motions are symmetric with respect to the model towing direction. These symmetry considerations are also true for pure yaw test, but are not appropriate for yaw and drift test due to its asymmetric motion (Fig. 4d). Hence, D_{asym} in equation (5.35) can be redefined for pure sway and pure yaw data as

$$D_{asym} = |r - r_{FS}| \tag{5.36}$$

where r_{FS} is the corrected data by dropping the odd- or even-order FS harmonics according to their symmetry- or anti-symmetry characteristics of the variable, respectively. Then, B_{asym} for pure sway and pure yaw data are defined as per the equations (5.34).

Evaluation results are summarized in Table 5-10, including $\langle D_{asym} \rangle$, $\langle U_r \rangle$, $\langle B_{asym} \rangle$, and $\langle U_{T_1} \rangle$ values, defined similarly as (5.32), presented in % of D_{rm} value. D_{rm} is the absolute value of r_m for static drift, whereas for pure sway and pure yaw, D_{rm} is the absolute period-mean value of X, z, and θ and the dynamic range of r_{FS} for Y and N. Herein, the results are presented in the order of X, Y, N, z, and θ data and in averages of the three Fr cases for static drift and pure yaw. In general, B_{asym} is large for X compared to those for Y and N, and also large for z and θ. For static drift data, B_{asym} is 8%, 0%, 0%, 4%, 114%, respectively, where the value for X is considerably larger than the U_r estimation, 2%. By including the B_{asym}, the total uncertainty U_{T_1} values are evaluated as 9%, 4%, 3%, 8%, and 126%, respectively. For pure sway, $\langle B_{asym} \rangle$ is 6%, 5%, 0%, 12%, and 0%, respectively, with $\langle U_{T_1} \rangle$ 10%, 5%, 2%, 14%, and 28%, respectively. For pure yaw, $\langle B_{asym} \rangle$ is 5%, 2%, 1%, 30%, and 24%, respectively, with $\langle U_{T_1} \rangle$ 10%, 7%, 2%, 32%, 57%, respectively.

5.1.6 UA Comparisons between Facilities

UA results for three facilities data, IIHR, FORCE, and INSEAN, are compared. The facilities have different dimensions (L×B×D), 100m×3.048m×3.048m,

240m×12m×4.4m, and 500m×12.5m×6.5m, respectively, and different model size, 3.048m, 4.002m, and 5.720m, respectively. Results are summarized in Table 5-11, including the contributions of bias B_r^2 and precision P_r^2 limits presented in % U_r^2 and the total uncertainty U_r presented in % |r| values. The |r| is defined as the X, Y, or N value at $\beta = 10°$ for static drift, the value at $v = v_{max}$ for pure sway, and $r = r_{max}$ for both pure yaw and yaw and drift, respectively. Herein the results are presented in the order of IIHR, FORCE, and INSEAN, and in averages for all variables and Fr cases where applicable, otherwise mentioned. In general, B_r is predominant, 90%, 69%, and 97% for static drift, respectively, and 67%, 95%, and 66% for dynamic tests, respectively, whereas P_r is dominant or both B_r and P_r are large for several cases such as the dynamic tests X for IIHR, static drift N for FORCE, and pure yaw N for INSEAN. Static drift U_r is small, 3% for all facilities data, whereas dynamic test U_r is relatively larger than static drift, 5%, 2%, and 2% for pure sway, respectively, 10%, 6%, and 4% for pure yaw, respectively, and 5%, 4%, and 3% for yaw and drift, respectively.

The U_r (% |r|) values are compared between facilities data observing the data trends with the model length and with Fr. First, U_r values are plotted in Fig. 5-4 against the model length, scaled with the smallest value, i.e., L = 1.0, 1.3, and 1.9, for IIHR, FORCE, and INSEAN, respectively. Although data exhibit scatters, mean values show trends with model length. Static drift mean values in Fig. 5-4 (a) are almost independent of model length, 3.1%, 3.3%, and 28%, respectively, whereas mean values of dynamic tests in Fig. 5-4 (b) decrease with model length, 8.3%, 4.8%, and 3.2%, respectively. Next, static drift and pure yaw U_r values are plotted in Fig. 5-5 (a) and (b), respectively, against Fr numbers, 0.138, 0.280, and 0.410. Again, the U_r values show scatters, while the mean values exhibit a rather clear Fr trend; decreasing with Fr, 4.3%, 2.6%, and 2.3% for static drift, and 11.3%, 4.6%, and 4.2% for pure yaw.

The asymmetry bias B_{asym} is evaluated for FORCE and INSEAN data, and the $\langle U_r \rangle$, $\langle B_{asym} \rangle$, and $\langle U_{T_1} \rangle$ values are presented in % D_{r_m} similarly as defined in Section

5.1.5, summarized in Table 5-12. Results are presented herein in the order of X, Y, and N, and for static drift and pure yaw data in averages of all Fr cases. The $\langle B_{asym} \rangle$ values are evaluated as, for static drift 1%, 0%, and 1% for FORCE, respectively, and 8%, 0%, and 0% for INSEAN, respectively; for pure sway 0%, 0%, and 0% for FORCE, respectively, and 11%, 0%, and 0% for INSEAN, respectively; and for pure yaw 0%, 0%, and 1% for FORCE, and 6%, 2%, and 0% for INSEAN, respectively. The overall mean $\langle B_{asym} \rangle$ values are small for FORCE facility data, 0%, 0%, and 1%, respectively, but relatively large for INSEAN, 8%, 1%, and 0%, respectively, where the INSEAN exhibit similar $\langle B_{asym} \rangle$ values as IIHR, 7%, 2%, and 0%, respectively, as previously shown in Table 5-10. For IIHR and INSEAN, the $\langle B_{asym} \rangle$ values for X data are evaluated as larger than the total uncertainty limits $\langle U_r \rangle$ values, 5% and 2%, respectively, and are combined into $\langle U_{T_1} \rangle$ as per (30), 10% and 9%, respectively.

5.1.7 Facility Bias

UA results show reasonable uncertainty levels in general, nevertheless for several cases, deviations of data from the facility-mean value, $\bar{r}$, exceed the total uncertainty estimations for each facility data, particularly for many cases for X. Those deviations of the data are considered to be from using different model size, different model manufactures, different towing tank dimensions, different water properties such as density, different towing carriage driving mechanisms, different PMM generators, different measurement systems, and so on, which cannot be accounted for each individual facility UA procedures. The facility biases or certification intervals of facilities are estimated using the M×N-order testing method as per Stern et al. (2005). The method is a statistical approach for assessing probabilistic confidence intervals with the mean facility data as reference values for M facilities with N repeat tests (N-order level testing) under the assumptions of normal distribution for the sample population X_i, 95% confidence level, M ≥ 10, and N

≥ 10. Herein, M = 3 and N = 12 are used. Although the number of facilities, M = 3, is minimal, the results show usefulness of the approach as discussed by Stern.

For the mean facility data $\bar{X}$, where X is either X, Y, or N of individual facility N-order test, the uncertainty $U_{\bar{X}}$ in $\bar{X}$ is the RSS of the bias limit $B_{\bar{X}}$ and the precision limit $P_{\bar{X}}$, which are the average RSS's of the M bias limits B_{X_i} and M precision limits P_{X_i}, respectively. The subscript i represents each facility data. Comparing the difference $D_i = X_i - \bar{X}$ with its uncertainty $U_{D_i}^2 = U_{X_i}^2 + U_{\bar{X}}^2$, if the absolute value of D_i is less than U_{D_i} i.e., $|D_i| \leq U_{D_i}$, then the individual facility is certified at interval U_{D_i}, whereas if $|D_i| > U_{D_i}$ then the facility bias B_{FB_i} which is defined as

$$B_{FB_i}^2 = D_i^2 - U_{D_i}^2 \tag{5.37}$$

with total uncertainty U_{T_2} as per equation (5.31). Interval certification provides additional confidence in measurements accuracy for certified facilities since it validates X_i and accounts for $U_{\bar{X}}$ in assessing the level of certification, and an improved estimate U_{T_2} for noncertified facilities accounting for facility biases.

B_{FB} is evaluated at $\beta = 10°$ for static drift test, whereas for dynamic tests B_{FB} is evaluated at $v = v_{max}$ for pure sway and $r = r_{max}$ for pure yaw and yaw and drift, respectively. Evaluation results of B_{FB} is summarized in Table 5-13 for IIHR data including $U_{\bar{X}}$, $|D_i|$, U_{D_i}, and U_{T_2}, and in Table 5-14 for FORCE and INSEAN data including $|D_i|$, U_{D_i}, and U_{T_2}, respectively, with all data presented in % $|\bar{X}|$ values. Herein, results are presented in the order of X, Y, and N and in averages for Fr cases where applicable. For static drift, B_{FB} is about 0%, 0%, and 1% for IIHR, respectively, about 0%, 1%, and 1% for FORCE, respectively, and about 3%, 4%, and 3% for INSEAN, respectively. Accordingly, IIHR and FORCE data are certified within certificate interval U_{D_i} about 11%, 4%, and 4% for IIHR, respectively, and about 8%, 3%, and 3% for FORCE, respectively, whereas U_{T_2} for INSEAN data is estimated at about 11%, 5%, and 5%, respectively, in-

creased from the U_X estimates about 9%, 3%, and 3%, respectively, by including the B_{FB}. For dynamic test data, in general, most of IIHR data are certified but with relatively large certificate intervals U_D about 3% ~ 30%, whereas FORCE and INSEAN data for several cases are uncertified with facility biases B_{FB} about 2% ~ 7%.

Table 5-1 Sensitivity coefficients of the bias limits for dynamic tests.

θ	B_X	B_Y	B_N
θ_L	$\dfrac{-2\left(F_x+m(\dot{u}-rv-x_G r^2-y_G\dot{r})\right)}{\rho(u^2+v^2)L^2T}$	$\dfrac{-2\left(F_y+m(\dot{v}+ru-y_G r^2+x_G\dot{r})\right)}{\rho(u^2+v^2)L^2T}$	$\dfrac{-4\left(M_z+I_z\dot{r}+m\left(x_G(\dot{v}+ru)-y_G(\dot{u}-rv)\right)\right)}{\rho(u^2+v^2)L^3T}$
θ_T	$\dfrac{-2\left(F_x+m(\dot{u}-rv-x_G r^2-y_G\dot{r})\right)}{\rho(u^2+v^2)LT^2}$	$\dfrac{-2\left(F_y+m(\dot{v}+ru-y_G r^2+x_G\dot{r})\right)}{\rho(u^2+v^2)LT^2}$	$\dfrac{-2\left(M_z+I_z\dot{r}+m\left(x_G(\dot{v}+ru)-y_G(\dot{u}-rv)\right)\right)}{\rho(u^2+v^2)L^2T^2}$
θ_{x_G}	$\dfrac{-2mr^2}{\rho(u^2+v^2)LT}$	$\dfrac{2m\dot{r}}{\rho(u^2+v^2)LT}$	$\dfrac{2m(\dot{v}+ru)}{\rho(u^2+v^2)L^2T}$
θ_{y_G}	$\dfrac{-2m\dot{r}}{\rho(u^2+v^2)LT}$	$\dfrac{-2mr^2}{\rho(u^2+v^2)LT}$	$\dfrac{-2m(\dot{u}-rv)}{\rho(u^2+v^2)L^2T}$
θ_m	$\dfrac{2(\dot{u}-rv-x_G r^2-y_G\dot{r})}{\rho(u^2+v^2)LT}$	$\dfrac{2(\dot{v}+ru-y_G r^2+x_G\dot{r})}{\rho(u^2+v^2)LT}$	$\dfrac{2\left(x_G(\dot{v}+ru)-y_G(\dot{u}-rv)\right)}{\rho(u^2+v^2)L^2T}$
θ_{I_z}	-	-	$\dfrac{2\dot{r}}{\rho(u^2+v^2)L_{PP}^2T_m}$
θ_ρ	$\dfrac{-2\left(F_x+m(\dot{u}-rv-x_G r^2-y_G\dot{r})\right)}{\rho^2(u^2+v^2)LT}$	$\dfrac{-2\left(F_y+m(\dot{v}+ru-y_G r^2+x_G\dot{r})\right)}{\rho^2(u^2+v^2)LT}$	$\dfrac{-2\left(M_z+I_z\dot{r}+m\left(x_G(\dot{v}+ru)-y_G(\dot{u}-rv)\right)\right)}{\rho^2(u^2+v^2)L^2T}$
θ_u	$\dfrac{-4u\left(F_x+m(\dot{u}-rv-x_G r^2-y_G\dot{r})\right)}{\rho(u^2+v^2)LT}$	$\dfrac{2}{\rho(u^2+v^2)LT}\left[mr-\dfrac{2u\left(F_y+m(\dot{v}+ru-y_G r^2+x_G\dot{r})\right)}{(u^2+r^2)}\right]$	$\dfrac{2}{\rho(u^2+v^2)L^2T}\left[mx_G r-\dfrac{2u\left(M_z+I_z\dot{r}+m\left(x_G(\dot{v}+ru)-y_G(\dot{u}-rv)\right)\right)}{(u^2+r^2)}\right]$
θ_v	$\dfrac{2}{\rho(u^2+v^2)LT}\left[-mr-\dfrac{2v\left(F_x+m(\dot{u}-rv-x_G r^2-y_G\dot{r})\right)}{(u^2+v^2)}\right]$	$\dfrac{4v\left(F_y+m(\dot{v}+ru-y_G r^2+x_G\dot{r})\right)}{\rho(u^2+v^2)LT}$	$\dfrac{2}{\rho(u^2+v^2)L^2T}\left[my_G r-\dfrac{2v\left(M_z+I_z\dot{r}+m\left(x_G(\dot{v}+ru)-y_G(\dot{u}-rv)\right)\right)}{(u^2+r^2)}\right]$
θ_r	$\dfrac{-2m(v+2x_G r)}{\rho(u^2+v^2)LT}$	$\dfrac{2m(u-2y_G r)}{\rho(u^2+v^2)LT}$	$\dfrac{2(x_G u+y_G v)}{\rho(u^2+v^2)L^2T}$
$\theta_{\dot{u}}$	$\dfrac{2m}{\rho(u^2+v^2)LT}$	-	$\dfrac{-2my_G}{\rho(u^2+v^2)L^2T}$
$\theta_{\dot{v}}$	-	$\dfrac{2m}{\rho(u^2+v^2)LT}$	$\dfrac{2mx_G}{\rho(u^2+v^2)L^2T}$
$\theta_{\dot{r}}$	$\dfrac{-2my_G}{\rho(u^2+v^2)LT}$	$\dfrac{2mx_G}{\rho(u^2+v^2)LT}$	$\dfrac{2I_z}{\rho(u^2+v^2)L^2T}$
θ_F	$\dfrac{2}{\rho(u^2+v^2)LT}$	$\dfrac{2}{\rho(u^2+v^2)LT}$	$\dfrac{2}{\rho(u^2+v^2)L^2T}$

Table 5-2. Sensitivity coefficients of the bias limits for static drift test.

θ	B_X	B_Y	B_N
$\theta_{L_{PP}}$	$\dfrac{-2F_x}{\rho U_C^2 L^2 T}$	$\dfrac{-2F_y}{\rho U_C^2 L^2 T}$	$\dfrac{-2M_z}{\rho U_C^2 L^3 T}$
θ_{T_m}	$\dfrac{-2F_x}{\rho U_C^2 L T^2}$	$\dfrac{-2F_y}{\rho U_C^2 L T^2}$	$\dfrac{-2M_z}{\rho U_C^2 L^2 T^2}$
θ_ρ	$\dfrac{-2F_x}{\rho^2 U_C^2 L T}$	$\dfrac{-2F_y}{\rho^2 U_C^2 L T}$	$\dfrac{-2M_z}{\rho U_C^2 L^2 T}$
θ_{U_C}	$\dfrac{-4F_x}{\rho U_C^3 L T}$	$\dfrac{-4F_y}{\rho U_C^3 L T}$	$\dfrac{-4M_z}{\rho U_C^3 L^2 T}$
θ_F	$\dfrac{2}{\rho U_C^2 L T}$	$\dfrac{2}{\rho U_C^2 L T}$	$\dfrac{2}{\rho U_C^2 L^2 T}$

Table 5-3. Polynomial models for measured force/moment, $\tilde{F}$.

Pure sway:

$$\tilde{F}_x = A_0 + A_u u + A_v v + A_r r + A_{vv} v^2 + A_{\dot{u}} \dot{u} + A_{\dot{v}} \dot{v} + A_{\dot{r}} \dot{r}$$

$$\tilde{F}_y = B_0 + B_u u + B_v v + B_r r + B_{v|v|} v|v| + B_{\dot{u}} \dot{u} + B_{\dot{v}} \dot{v} + B_{\dot{r}} \dot{r}$$

$$\widetilde{M}_z = C_0 + C_u u + C_v v + C_r r + C_{v|v|} v|v| + C_{\dot{u}} \dot{u} + C_{\dot{v}} \dot{v} + C_{\dot{r}} \dot{r}$$

Pure yaw:

$$\tilde{F}_x = A_0 + A_u u + A_v v + A_r r + A_{rr} r^2 + A_{\dot{u}} \dot{u} + A_{\dot{v}} \dot{v} + A_{\dot{r}} \dot{r}$$

$$\tilde{F}_y = B_0 + B_u u + B_v v + B_r r + B_{rrr} r^3 + B_{\dot{u}} \dot{u} + B_{\dot{v}} \dot{v} + B_{\dot{r}} \dot{r}$$

$$\widetilde{M}_z = C_0 + C_u u + C_v v + C_r r + C_{rrr} r^3 + C_{\dot{u}} \dot{u} + C_{\dot{v}} \dot{v} + C_{\dot{r}} \dot{r}$$

Yaw and drift:

$$\tilde{F}_x = A_0 + A_u u + A_v v + A_r r + A_{uu} u^2 + A_{vv} v^2 + A_{rr} r^2 + A_{uv} uv + A_{\dot{u}} \dot{u} + A_{\dot{v}} \dot{v} + A_{\dot{r}} \dot{r}$$

$$\tilde{F}_y = B_0 + B_u u + B_v v + B_r r + B_{v|v|} v|v| + B_{uv} uv + B_{v|r|} v|r| + B_{r|v|} r|v| + B_{rrr} r^3 + B_{vrr} vr^2 + B_{rvv} rv^2$$
$$+ B_{\dot{u}} \dot{u} + B_{\dot{v}} \dot{v} + B_{\dot{r}} \dot{r}$$

$$\widetilde{M}_z = C_0 + C_u u + C_v v + C_r r + C_{v|v|} v|v| + C_{uv} uv + C_{v|r|} v|r| + C_{r|v|} r|v| + C_{rrr} r^3 + C_{vrr} vr^2 + C_{rvv} rv^2$$
$$+ C_{\dot{u}} \dot{u} + C_{\dot{v}} \dot{v} + C_{\dot{r}} \dot{r}$$

Table 5-4 Bias limits of global variables.

Var. (x)	L (m)	T (m)	x_G (m)	y_G (m)	m (Kg)	I_z (Kg·m²)	ρ (Kg/m³)	U_C (m/s)
D_x	3.048	0.132	0.016	0.0	82.55 (83.35)	49.79 (44.48)	998.1	2.241
B_x	0.002	0.001	0.005	0.002	0.11 (0.08)	1.84 (1.89)	0.041	0.010
$\%D_x$	0.07	0.7	31.3	-	0.1 (0.1)	3.7 (4.2)	0.004	0.5

( ): values for fixed conditions.

Table 5-5 Bias limits of PMM motion parameters for dynamic tests ($Fr = 0.280$).

					x	S_{mm} (mm)	N (rpm)	t (sec)	β (°)	ψ_{max} (°)
				$\langle B_\chi \rangle$	D_x	250	15	0.01	30	30
Var. (χ)	Unit	Test type	D_χ		B_x	0.5	0.0006	0.001	0.22	0.22
				$(\%D_\chi)$	$\%D_x$	0.2	0.0	10.0	0.7	0.7
						Elemental bias B_x contributions $\frac{\langle \theta_x^2 B_x^2 \rangle}{\langle B_x^2 \rangle}$ (%)				
v_{PMM}	(m/s)	Pure sway	0.5359	0.1		**92.7**	0.8	6.6	-	-
		Pure yaw	0.5529	0.1		**92.2**	0.8	7.0	-	-
		Yaw & drift	0.5558	0.1		**92.2**	0.8	7.0	-	-
$\dot{v}_{PMM}$	(m/s²)	Pure sway	0.4512	0.1		**92.6**	0.8	6.6	-	-
		Pure yaw	0.4646	0.1		**92.1**	0.9	7.0	-	-
		Yaw & drift	0.4671	0.1		**92.1**	0.9	7.0	-	-
ψ	(°)	Pure sway	0.1	222.1		-	0.0	0.0	**67.0**	**33.0**
		Pure yaw	20.4	1.3		-	0.0	0.1	**67.0**	**32.9**
		Yaw & drift	20.4	1.3		-	0.0	0.2	**66.9**	**32.9**
r_{PMM}	(rad/s)	Pure sway	0.0032	63.3		-	0.0	0.0	-	**100.0**
		Pure yaw	0.3005	0.7		-	0.0	0.2	-	**99.8**
		Yaw & drift	0.3007	0.7		-	0.1	0.6	-	**99.3**
$\dot{r}_{PMM}$	(rad/s²)	Pure sway	0.0056	30.9		-	0.0	0.0	-	**100.0**
		Pure yaw	0.2545	0.7		-	0.0	0.2	-	**99.8**
		Yaw & drift	0.2526	0.7		-	0.1	0.6	-	**99.3**

Var. (X)	Unit	Test type	D_X	$\langle B_X \rangle$ $(\%D_X)$	Elemental bias B_x contributions $\frac{\langle \theta_X^2 B_X^2 \rangle}{\langle B_X^2 \rangle}$ (%)					
					U_C	v_{PMM}	$\dot{v}_{PMM}$	ψ	r_{PMM}	$\dot{r}_{PMM}$
u	(m/s)	Pure sway	1.5177†	0.7	**99.1**	0.0	-	0.9	-	-
		Pure yaw	1.5397†	0.7	**100.0**	0.0	-	0.0	-	-
		Yaw & drift	1.5151†	0.7	**98.4**	0.0	-	1.6	-	-
v	(m/s)	Pure sway	0.5382	1.3	0.0	0.7	-	**99.3**	-	-
		Pure yaw	0.0090	81.6	3.0	0.7	-	**96.4**	-	-
		Yaw & drift	0.2672†	2.8	8.2	0.6	-	**91.1**	-	-
r	(rad/s)	Pure sway	0.0032	63.3	-	-	-	-	**100.0**	-
		Pure yaw	0.3005	0.7	-	-	-	-	**100.0**	-
		Yaw & drift	0.3007	0.7	-	-	-	-	**100.0**	-
$\dot{u}$	(m/s²)	Pure sway	0.0006	115.0	0.0	0.0	0.0	**83.5**	16.5	-
		Pure yaw	0.0423	0.3	**63.2**	**16.9**	**17.1**	2.6	0.2	-
		Yaw & drift	0.0418	1.4	**10.1**	0.6	2.5	0.1	**86.6**	-
$\dot{v}$	(m/s²)	Pure sway	0.4539	0.1	0.0	0.0	**100.0**	0.0	0.0	-
		Pure yaw	0.0161	6.8	**80.8**	0.0	**18.9**	0.3	0.0	-
		Yaw & drift	0.0196	5.6	**77.4**	0.0	**18.1**	4.5	0.0	-
$\dot{r}$	(rad/s²)	Pure sway	0.0056	30.9	-	-	-	-	-	**100.0**
		Pure yaw	0.2545	0.7	-	-	-	-	-	**100.0**
		Yaw & drift	0.2526	0.7	-	-	-	-	-	**100.0**

† period mean values; - not applicable.

Table 5-6 Bias limits of measured forces and moment (B_F).

Test	F	Unit	Fr	D_F	$\langle B_F \rangle$ (%D_F)	β	align	ref	fit	u	v	r	$\dot{u}$	$\dot{v}$	$\dot{r}$	t
Static drift	F_x	(N)	0.138	2.4	0.5	**47.4**	0.9	0.7	**51.0**	-	-	-	-	-	-	-
			0.280	10.9	1.1	**91.8**	1.7	0.0	6.5	-	-	-	-	-	-	-
			0.410	32.5	0.8	**88.0**	1.6	0.0	10.4	-	-	-	-	-	-	-
	F_y	(N)	0.138	6.1	2.8	**97.9**	1.8	0.0	0.3	-	-	-	-	-	-	-
			0.280	28.5	2.9	**97.0**	1.8	0.0	1.2	-	-	-	-	-	-	-
			0.410	69.3	3.5	**97.2**	1.8	0.0	1.0	-	-	-	-	-	-	-
	M_z	(Nm)	0.138	8.7	2.6	**95.2**	1.7	1.5	1.5	-	-	-	-	-	-	-
			0.280	44.1	2.5	**96.8**	1.8	0.1	1.4	-	-	-	-	-	-	-
			0.410	108.5	3.1	**97.3**	1.8	0.0	0.9	-	-	-	-	-	-	-
Pure sway	F_x	(N)	0.280	11.50	0.7	-	-	0.0	**12.9**	0.5	**86.4**	0.0	0.0	0.1	0.0	0.0
	F_y	(N)		86.08	1.0	-	-	0.0	1.3	0.0	**97.8**	0.0	0.0	0.8	0.0	0.1
	M_z	(Nm)		94.46	1.4	-	-	0.0	0.5	0.0	**99.4**	0.0	0.0	0.0	0.0	0.0
Pure yaw	F_x	(N)	0.138	2.13	0.8	-	-	0.3	**23.0**	0.0	**32.5**	12.8	5.9	**25.3**	0.2	0.0
			0.280	9.00	0.6	-	-	0.0	**19.1**	0.0	0.0	11.8	1.8	**67.0**	0.1	0.1
			0.410	27.49	0.4	-	-	0.0	**53.7**	0.0	3.7	27.0	5.0	9.8	0.0	0.7
	F_y	(N)	0.138	11.19	0.8	-	-	0.0	0.4	0.0	0.0	**96.2**	0.0	0.1	3.2	0.0
			0.280	54.36	0.7	-	-	0.0	2.0	0.0	0.1	**96.4**	0.0	1.1	0.3	0.1
			0.410	118.49	0.8	-	-	0.0	1.7	0.0	0.1	**95.9**	0.0	0.6	1.4	0.3
	M_z	(Nm)	0.138	10.25	0.9	-	-	8.7	1.8	0.0	0.0	**53.2**	0.0	0.0	**36.2**	0.0
			0.280	47.67	0.8	-	-	0.6	2.0	0.0	0.0	**72.7**	0.0	0.7	**24.0**	0.1
			0.410	131.07	0.9	-	-	0.1	1.3	0.0	0.1	**74.7**	0.0	0.1	**23.4**	0.3
Yaw & drift	F_x	(N)	0.280	10.23	1.5	-	-	0.0	4.0	**55.5**	1.3	**29.2**	8.5	1.2	0.2	0.1
	F_y	(N)		67.48	1.2	-	-	0.0	3.0	0.0	**54.8**	38.6	0.0	3.2	0.3	0.1
	M_z	(Nm)		66.37	1.4	-	-	0.1	2.8	3.1	**62.1**	24.7	0.0	3.5	3.8	0.0

Elemental bias $B_{F,x}$ contribution $\frac{\langle B_{F,x}^2 \rangle}{\langle B_F^2 \rangle}$ (%)

- not applicable.

Table 5-7 Total bias limits of non-dimensional forces and moment (B_r).

Test	r	Fr	Elemental bias B_x contributions $\frac{\langle \theta_x^2 B_x^2 \rangle}{\langle B_r^2 \rangle}$ (%)													
			L	T	x_G	y_G	m	I_z	ρ	$u^\dagger$	v	r	$\dot{u}$	$\dot{v}$	$\dot{r}$	F
Static drift	X	0.138	0.1	7.0	-	-	-	-	0.0	**89.7**	-	-	-	-	-	3.3
		0.280	0.1	**15.8**	-	-	-	-	0.0	**49.4**	-	-	-	-	-	**34.7**
		0.410	0.2	**26.9**	-	-	-	-	0.0	**39.7**	-	-	-	-	-	**33.2**
	Y	0.138	0.0	3.7	-	-	-	-	0.0	**46.7**	-	-	-	-	-	**49.6**
		0.280	0.0	5.3	-	-	-	-	0.0	**16.6**	-	-	-	-	-	**78.0**
		0.410	0.0	4.2	-	-	-	-	0.0	6.2	-	-	-	-	-	**89.5**
	N	0.138	0.1	2.7	-	-	-	-	0.0	**34.0**	-	-	-	-	-	**63.3**
		0.280	0.1	3.2	-	-	-	-	0.0	**10.1**	-	-	-	-	-	**86.6**
		0.410	0.1	2.4	-	-	-	-	0.0	3.5	-	-	-	-	-	**94.1**
Pure sway	X	0.280	0.0	5.1	0.0	0.0	0.0	-	0.0	**86.1**	0.1	0.4	2.6	-	0.0	5.6
	Y		0.0	2.9	0.0	0.0	0.0	-	0.0	8.8	0.6	8.4	-	0.2	0.0	**79.0**
	N		0.1	2.7	0.2	0.0	0.0	0.0	0.0	8.4	0.1	0.0	0.0	0.0	0.4	**88.0**
Pure yaw	X	0.138	0.1	**14.0**	0.1	1.1	0.0	-	0.0	**57.3**	11.2	0.0	0.7	-	0.0	15.5
		0.280	0.0	5.1	0.0	0.3	0.0	-	0.0	**86.6**	3.8	0.0	0.1	-	0.0	4.1
		0.410	0.0	2.7	0.0	0.1	0.0	-	0.0	**95.5**	1.0	0.0	0.0	-	0.0	0.6
	Y	0.138	0.0	0.2	0.5	0.0	0.1	-	0.0	**18.1**	0.0	**28.8**	-	9.2	0.0	**43.0**
		0.280	0.0	0.6	0.5	0.0	0.1	-	0.0	8.7	0.0	**28.5**	-	3.3	0.0	**58.2**
		0.410	0.0	0.5	0.6	0.0	0.1	-	0.0	3.3	0.0	**29.9**	-	1.9	0.0	**63.7**
	N	0.138	0.1	2.7	1.6	0.0	0.0	10.6	0.0	**33.7**	0.0	0.0	0.0	0.0	4.8	**46.4**
		0.280	0.2	5.9	2.3	0.0	0.0	11.2	0.0	**17.7**	0.0	0.0	0.0	0.0	3.8	**58.8**
		0.410	0.2	5.1	1.2	0.0	0.0	9.1	0.0	7.3	0.0	0.0	0.0	0.0	4.5	**72.7**
Yaw & drift	X	0.280	0.0	4.4	0.0	0.2	0.0	-	0.0	**70.9**	2.6	1.8	2.1	-	0.0	**17.8**
	Y		0.0	6.6	0.1	0.0	0.0	-	0.0	**21.7**	1.8	7.6	-	0.9	0.0	**61.2**
	N		0.3	**10.3**	0.3	0.0	0.0	1.7	0.0	**29.4**	0.5	0.0	0.0	0.0	0.6	**56.9**

$^\dagger U_C$ for static drift test; - not applicable.

Table 5-8 Identifications of primary bias sources and propagations.

Test	Bias	Test type[1]	Primary biases and propagations	Bias source
Static	$B_X, B_Y,$ B_N	SD	B_{U_C} $B_F \leftarrow B_{F,\beta} \leftarrow B_\beta$	U_C, β
Dyanmic	B_X	PS,PY,YD	$B_u \leftarrow B_{U_C}$	U_C
	B_Y, B_N	PS	$B_F \leftarrow B_{F,v} \leftarrow B_v \leftarrow B_\psi \leftarrow B_\beta, B_{\psi_{max}}$	β, ψ_{max}
		PY	$B_F \leftarrow B_{F,r} \leftarrow B_r \leftarrow B_{r_{PMM}} \leftarrow B_{\psi_{max}}$	
		YD	$B_F \leftarrow B_{F,v}/B_{F,r} \leftarrow B_v/B_r \leftarrow B_\psi/B_{r_{PMM}} \leftarrow B_\beta, B_{\psi_{max}}$	

1) SD = static drift; PS = pure sway; PY = pure yaw; YD = yaw and drift.

Table 5-9 Summary of UA results.

Test	R	Fr	D_r	$\langle B_\mathrm{r} \rangle$	$\dfrac{\langle B_\mathrm{r}^2 \rangle}{\langle U_\mathrm{r}^2 \rangle}$	$\langle P_\mathrm{r} \rangle$	$\dfrac{\langle P_\mathrm{r}^2 \rangle}{\langle U_\mathrm{r}^2 \rangle}$	$\langle U_\mathrm{r} \rangle$
		[-]	[-]	(%D_r)	(%)	(%D_r)	(%)	(%D_r)
Static drift	X	0.138	0.021	2.9	**95.9**	0.6	4.1	2.9
		0.280	0.023	2.0	**96.6**	0.3	3.4	1.9
		0.410	0.033	1.5	**69.3**	1.0	30.7	1.8
	Y	0.138	0.054	3.9	**82.7**	1.8	17.3	4.4
		0.280	0.061	3.3	**95.1**	0.8	4.9	3.4
		0.410	0.070	3.7	**99.6**	0.2	0.4	3.7
	N	0.138	0.025	3.3	**80.2**	1.6	19.8	3.6
		0.280	0.031	2.7	**94.5**	0.6	5.5	2.8
		0.410	0.036	3.2	**99.6**	0.2	0.4	3.2
	z (10^{-2})	0.138	0.054	6.1	**76.9**	3.3	23.1	6.9
		0.280	0.296	1.1	**66.6**	0.8	33.4	1.4
		0.410	0.726	0.5	15.8	1.1	**84.2**	1.1
	θ (°)	0.138	0.020	197.6	**99.9**	7.3	0.1	197.7
		0.280	-0.152	26.4	**99.9**	0.9	0.1	26.4
		0.410	0.217	18.4	**88.9**	6.5	11.1	19.6
Pure sway	X	0.280	0.024	3.4	24.8	5.8	**75.2**	4.7
	Y		0.133	1.6	**63.0**	1.2	37.0	2.0
	N		0.065	1.5	**93.6**	0.4	6.4	1.6
	z (10^{-3})		1.928	1.7	11.3	4.7	**88.7**	5.0
	θ (°)		0.163	24.5	**77.0**	13.3	23.0	27.9
Pure yaw	X	0.138	0.018	2.0	3.7	10.3	**96.3**	10.5
		0.280	0.019	3.4	19.0	6.8	**81.0**	7.6
		0.410	0.027	4.6	**66.5**	3.2	33.5	5.7
	Y	0.138	0.026	4.7	36.2	6.7	**63.8**	8.3
		0.280	0.034	3.0	**74.4**	1.9	25.6	3.7
		0.410	0.039	3.3	**89.2**	1.2	10.8	3.6
	Y	0.138	0.025	1.6	**91.3**	0.5	8.7	1.7
		0.280	0.031	1.1	**81.1**	0.5	18.9	1.2
		0.410	0.040	1.2	**93.3**	0.3	6.7	1.2
	z (10^{-3})	0.138	0.294	11.2	**51.0**	10.8	49.0	15.6
		0.280	1.540	2.1	11.5	5.9	**88.5**	6.2
		0.410	4.944	0.7	15.6	1.5	**84.4**	1.7
	θ (°)	0.138	0.094	74.8	**99.3**	4.1	0.7	42.9
		0.280	0.127	31.5	**77.8**	16.8	22.2	35.7
		0.410	0.444	9.0	**86.8**	3.5	13.2	9.7
Yaw & drift	X	0.280	0.022	3.6	28.8	5.6	**71.2**	6.7
	Y		0.065	3.3	**80.1**	1.7	19.9	3.7
	N		0.045	1.9	**91.8**	0.6	8.2	2.0
	z (10^{-3})		3.224	1.0	11.7	2.8	**88.3**	3.0
	θ (°)		0.302	13.2	**75.8**	7.4	24.2	15.2

Table 5-10 Evaluation of asymmetry bias B_{asym}.

Test	r	Fr	D_{rm}	$\langle D_{asym} \rangle$ (%)	$\langle U_r \rangle$ (%)	$\langle B_{asym} \rangle$ (%)	$\langle U_{T_1} \rangle$ (%)
Static drift	X	0.138	0.0196	7.7	3.1	7.0	7.7
		0.280	0.0214	10.5	2.1	10.3	10.5
		0.410	0.0302	7.5	1.9	7.2	7.5
	Y	0.138	0.0524	2.0	4.5	0.0	4.5
		0.280	0.0619	0.4	3.3	0.0	3.3
		0.410	0.0715	1.8	3.6	0.0	3.6
	N	0.138	0.0250	0.0	3.7	0.0	3.7
		0.280	0.0313	0.6	2.8	0.0	2.8
		0.410	0.0365	0.8	3.1	0.0	3.1
	z (10^{-2})	0.138	0.046	18.3	8.1	16.4	18.3
		0.280	0.288	2.9	1.4	2.5	2.9
		0.410	0.714	1.7	1.2	1.2	1.7
	θ (°)	0.138	-0.050	140.2	79.5	115.5	140.2
		0.280	-0.212	28.5	18.9	21.4	28.5
		0.410	0.131	65.7	32.4	57.2	65.7
Pure sway	X	0.280	0.0245	9.0	6.7	6.1	10.0
	Y		0.1327	5.4	2.0	5.0	5.4
	N		0.0653	1.3	1.6	0.1	1.6
	z (10^{-3})		1.9284	13.2	5.0	11.9	13.5
	θ (°)		0.1631	4.1	27.9	0.0	27.9
Pure yaw	X	0.138	0.0185	10.3	10.5	5.7	12.9
		0.280	0.0189	9.5	7.6	5.9	10.4
		0.410	0.0274	6.6	5.7	4.2	7.7
	Y	0.138	0.0241	7.2	9.0	3.1	10.3
		0.280	0.0344	3.2	3.7	1.7	4.7
		0.410	0.0385	4.2	3.6	2.1	4.7
	N	0.138	0.0250	1.2	1.7	0.0	1.7
		0.280	0.0308	1.6	1.2	1.0	1.6
		0.410	0.0397	1.4	1.2	0.5	1.4
	z (10^{-3})	0.138	0.2820	74.0	16.3	71.1	74.8
		0.280	1.5398	18.2	6.2	16.7	18.5
		0.410	4.9434	3.4	1.7	2.9	3.6
	θ (°)	0.138	0.0433	95.1	92.5	52.0	115.5
		0.280	0.1270	33.4	35.7	17.1	42.9
		0.410	0.4442	9.0	9.7	3.7	11.1

Table 5-11 Comparisons of UA between facilities.

Test	r	Fr	IIHR $|r|$	B_r (%)	P_r (%)	U_r (%)	FORCE $|r|$	B_r (%)	P_r (%)	U_r (%)	INSEAN $|r|$	B_r (%)	P_r (%)	U_r (%)
Static drift[1]	X	0.138	0.0210	**95.9**	4.1	2.9	0.0174	**97.2**	2.8	11.3	0.0169	**92.8**	7.2	3.9
		0.280	0.0234	**96.6**	3.4	1.9	0.0195	**77.8**	22.2	3.4	0.0189	**94.1**	5.9	1.4
		0.410	0.0330	**69.3**	30.7	1.8	0.0278	**89.6**	10.4	1.6	0.0285	**91.2**	8.8	0.7
	Y	0.138	0.0538	**82.7**	17.3	4.4	0.0542	**79.0**	21.0	3.5	0.0552	**99.1**	0.9	3.1
		0.280	0.0611	**95.1**	4.9	3.4	0.0617	**74.2**	25.8	2.1	0.0626	**99.1**	0.9	3.3
		0.410	0.0703	**99.6**	0.4	3.7	0.0729	**69.6**	30.4	1.8	0.0717	**99.5**	0.5	3.9
	N	0.138	0.0251	**80.2**	19.8	3.6	0.0260	**69.2**	30.8	2.2	0.0261	**99.7**	0.3	3.4
		0.280	0.0310	**94.5**	5.5	2.8	0.0306	21.0	**79.0**	2.4	0.0309	**98.9**	1.1	3.1
		0.410	0.0361	**99.6**	0.4	3.2	0.0367	43.4	**56.6**	1.4	0.0363	**99.4**	0.6	2.8
Pure sway[2]	X	0.280	0.0292	35.2	**64.8**	5.8	0.0207	**98.1**	1.9	3.1	0.0197	46.6	**53.4**	1.3
	Y		0.0548	**73.3**	26.7	5.5	0.0565	**98.3**	1.7	1.8	0.0637	**66.0**	34.0	2.1
	N		0.0316	**98.0**	2.0	4.2	0.0306	**92.6**	7.4	1.5	0.0334	**73.0**	27.0	1.8
Pure yaw[3]	X	0.138	0.0224	4.0	**96.0**	9.9	0.0177	**97.6**	2.4	11.3	0.0156	**77.0**	23.0	4.2
		0.280	0.0215	20.8	**79.2**	7.4	0.0187	**98.8**	1.2	3.4	0.0168	**52.7**	47.3	1.7
		0.410	0.0303	**68.1**	31.9	5.6	0.0264	**98.0**	2.0	2.9	0.0249	**70.5**	29.5	0.9
	Y	0.138	0.0072	48.9	**51.1**	36.5	0.0114	**90.3**	9.7	15.8	0.0090	**70.1**	29.9	10.3
		0.280	0.0161	**88.0**	12.0	10.8	0.0178	**93.4**	6.6	5.5	0.0178	**85.5**	14.5	4.6
		0.410	0.0168	**90.1**	9.9	12.2	0.0176	**90.6**	9.4	3.5	0.0178	**86.2**	13.8	6.2
	N	0.138	0.0114	**94.7**	5.3	4.0	0.0114	**98.8**	1.2	7.3	0.0119	34.1	**65.9**	2.6
		0.280	0.0146	**90.0**	10.0	2.9	0.0140	**93.9**	6.1	3.3	0.0160	**59.6**	40.4	1.4
		0.410	0.0188	**94.1**	5.9	3.0	0.0186	**87.7**	12.3	1.4	0.0210	**61.4**	38.6	1.8
Yaw & drift[3]	X	0.280	0.0265	29.8	**70.2**	6.7	0.0234	**99.2**	0.8	5.8	0.0255	**67.6**	32.4	1.3
	Y		0.0470	**79.6**	20.4	4.7	0.0458	**89.0**	11.0	2.1	0.0469	**74.0**	26.0	3.5
	N		0.0135	**92.8**	7.2	4.9	0.0135	**98.0**	2.0	2.7	0.0134	**64.0**	36.0	4.4

[1] at $\beta = -10°$ for IIHR and $10°$ for FORCE and INSEAN; [2] at $v'(t) = v'_0$; [3] at $r'(t) = r'_0$.

Table 5-12 Evaluation of asymmetry bias B_{asym} (FORCE and INSEAN data).

	r	Fr	D_{r_m}	$\langle U_r \rangle$ (%)	$\langle B_{asym} \rangle$ (%)	$\langle U_{T_1} \rangle$ (%)	D_{r_m}	$\langle U_r \rangle$ (%)	$\langle B_{asym} \rangle$ (%)	$\langle U_{T_1} \rangle$ (%)
				FORCE				INSEAN		
Static drift	X	0.138	0.0185	10.6	0.0	10.6	0.0159	4.2	4.7	6.3
		0.280	0.0199	3.3	0.0	3.3	0.0174	1.5	11.4	11.5
		0.410	0.0285	1.5	1.9	2.5	0.0253	0.8	11.8	11.9
	Y	0.138	0.0539	3.5	0.0	3.5	0.0580	2.9	0.0	2.9
		0.280	0.0607	2.1	0.0	2.1	0.0620	3.3	0.0	3.3
		0.410	0.0718	1.9	0.0	1.9	0.0800	3.5	0.0	3.5
	N	0.138	0.0256	2.3	0.0	2.3	0.0228	2.9	0.0	2.9
		0.280	0.0297	2.5	1.7	3.0	0.0290	3.3	0.0	3.3
		0.410	0.0358	1.5	2.0	2.5	0.0390	2.6	0.0	2.6
Pure sway	X	0.280	0.0201	3.2	0.0	3.2	0.0184	1.2	11.1	11.3
	Y		0.1283	0.8	0.1	0.8	0.1392	0.9	0.0	0.9
	N		0.0615	0.8	0.4	0.9	0.0670	0.8	0.0	0.8
Pure yaw	X	0.138	0.0176	11.2	0.0	11.2	0.0153	3.9	6.0	7.8
		0.280	0.0188	3.4	0.1	3.4	0.0169	1.2	5.4	5.7
		0.410	0.0259	2.9	0.0	2.9	0.0246	0.8	6.4	6.5
	Y	0.138	0.0310	6.0	0.0	6.0	0.0226	4.3	3.8	6.2
		0.280	0.0368	2.7	0.0	2.7	0.0356	1.9	0.7	2.2
		0.410	0.0420	1.4	0.4	1.6	0.0434	2.0	0.4	2.1
	N	0.138	0.0242	3.1	1.5	3.8	0.0251	1.2	0.0	1.2
		0.280	0.0296	1.5	0.5	1.5	0.0329	0.7	0.0	0.7
		0.410	0.0394	0.5	1.4	1.5	0.0434	0.8	0.0	0.8

Table 5-13 Evaluation of facility bias B_{FB}.

Test	X	Fr	$\overline{X}$	$U_{\overline{X}}$ (%)	U_X (%)	$|D|$ (%)	U_D (%)	B_{FB} (%)	U_{T_2} (%)
Static drift	X	0.138	0.0180	4.9	8.4	8.9	9.7	0.0	8.4
		0.280	0.0196	5.2	11.5	9.4	12.6	0.0	10.9
		0.410	0.2800	4.5	8.0	7.9	9.2	0.0	8.0
	Y	0.138	0.0548	2.1	4.3	4.3	4.8	0.0	4.3
		0.280	0.0615	1.7	3.3	0.6	3.7	0.0	3.3
		0.410	0.0744	1.8	3.5	3.9	3.9	0.5	3.5
	N	0.138	0.0245	1.7	3.7	2.2	4.2	0.0	3.8
		0.280	0.0300	1.7	2.8	4.3	3.4	2.7	4.0
		0.410	0.0374	1.6	3.1	2.4	3.4	0.0	3.0
Pure sway	X	0.280	0.0225	5.4	7.6	20.6	9.3	18.3	19.8
	Y		0.0604	3.5	10.2	1.0	10.8	0.0	10.2
	N		0.0322	1.6	4.2	1.3	4.5	0.0	4.2
Pure yaw	X	0.138	0.0175	7.5	17.8	10.0	19.3	0.0	17.8
		0.280	0.0181	5.7	15.4	3.3	16.4	0.0	15.4
		0.410	0.0263	4.3	10.3	4.9	11.2	0.0	10.3
	Y	0.138	0.0096	13.0	27.2	13.0	30.2	0.0	27.3
		0.280	0.0175	4.2	9.9	3.0	10.7	0.0	9.9
		0.410	0.0180	4.5	11.3	2.8	12.2	0.0	3.2
	N	0.138	0.0117	3.5	3.9	0.9	5.3	0.0	3.9
		0.280	0.0150	1.7	3.3	0.4	3.7	0.0	3.3
		0.410	0.0196	1.3	2.8	2.0	3.1	0.0	2.8
Yaw & drift	X	0.280	0.0251	3.0	7.1	5.4	7.7	0.0	7.1
	Y		0.0465	2.1	4.7	0.7	5.2	0.0	4.7
	N		0.0135	2.4	4.9	0.0	5.5	0.0	5.0

Table 5-14 Evaluation of facility bias B_{FB} (FORCE and INSEAN data).

Test	r	Fr	FORCE U_X (%)	$|D|$ (%)	U_D (%)	B_{FB} (%)	U_{T_2} (%)	INSEAN U_X (%)	$|D|$ (%)	U_D (%)	B_{FB} (%)	U_{T_2} (%)
Static drift	X	0.138	10.9	2.8	12.0	0.0	10.9	5.6	11.7	7.4	9.0	10.6
		0.280	3.4	1.7	6.2	0.0	3.4	10.2	11.1	11.5	0.0	10.2
		0.410	2.5	1.8	5.2	0.0	2.5	10.8	9.6	11.7	0.0	10.8
	Y	0.138	3.4	1.6	4.0	0.0	3.4	3.1	5.9	3.7	4.6	5.5
		0.280	2.1	1.4	2.7	0.0	2.1	3.4	0.8	3.8	0.0	3.4
		0.410	1.8	3.5	2.6	2.4	3.0	3.8	7.5	4.2	6.2	7.3
	N	0.138	2.4	4.6	3.0	3.6	4.3	2.7	6.8	3.2	6.0	6.6
		0.280	3.0	1.0	3.4	0.0	3.0	3.2	3.3	3.6	0.0	3.2
		0.410	2.4	1.9	2.8	0.0	2.4	2.7	4.3	3.1	2.9	4.0
Pure sway	X	0.280	2.9	8.0	6.1	5.2	5.9	14.1	12.5	15.1	0.0	14.1
	Y		1.7	6.4	3.9	5.1	5.4	2.2	5.5	4.2	3.5	4.2
	N		1.5	5.1	2.2	4.6	4.8	1.9	3.8	2.5	2.9	3.4
Pure yaw	X	0.138	11.4	1.0	13.6	0.0	11.4	7.5	10.9	10.6	2.8	8.0
		0.280	3.5	3.4	6.7	0.0	3.5	6.4	6.7	8.6	0.0	6.4
		0.410	2.9	0.5	5.2	0.0	2.9	7.4	5.4	8.6	0.0	7.4
	Y	0.138	19.1	18.8	23.1	0.0	19.1	20.0	5.9	23.9	0.0	20.0
		0.280	5.6	1.4	7.0	0.0	5.6	5.4	1.6	6.8	0.0	5.4
		0.410	3.2	1.9	5.5	0.0	3.2	6.6	0.9	8.0	0.0	6.6
	N	0.138	9.5	2.6	10.1	0.0	9.5	2.6	1.7	4.4	0.0	2.6
		0.280	3.5	6.7	3.9	5.5	6.5	1.5	6.3	2.3	5.9	6.1
		0.410	1.9	5.3	2.3	4.7	5.1	1.9	7.3	2.3	6.9	7.2
Yaw & drift	X	0.280	5.3	6.8	6.1	3.1	6.2	1.2	1.4	3.2	0.0	1.2
	Y		2.1	1.6	2.9	0.0	2.1	3.5	0.8	4.1	0.0	3.5
	N		2.6	0.4	3.5	0.0	2.6	4.5	0.4	5.1	0.0	4.5
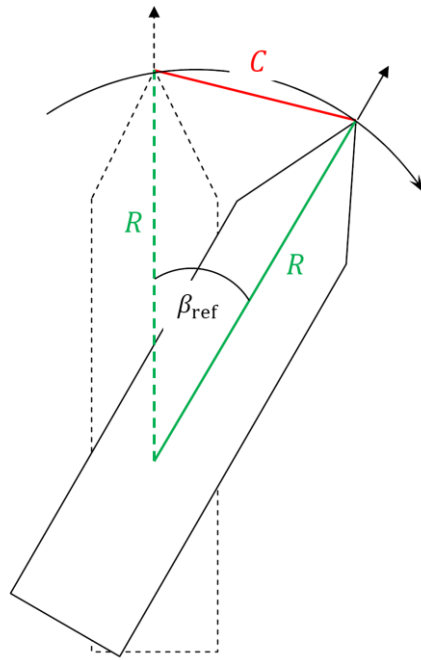
Figure 5-1 Definition of β_{ref} for drift angle calibration.
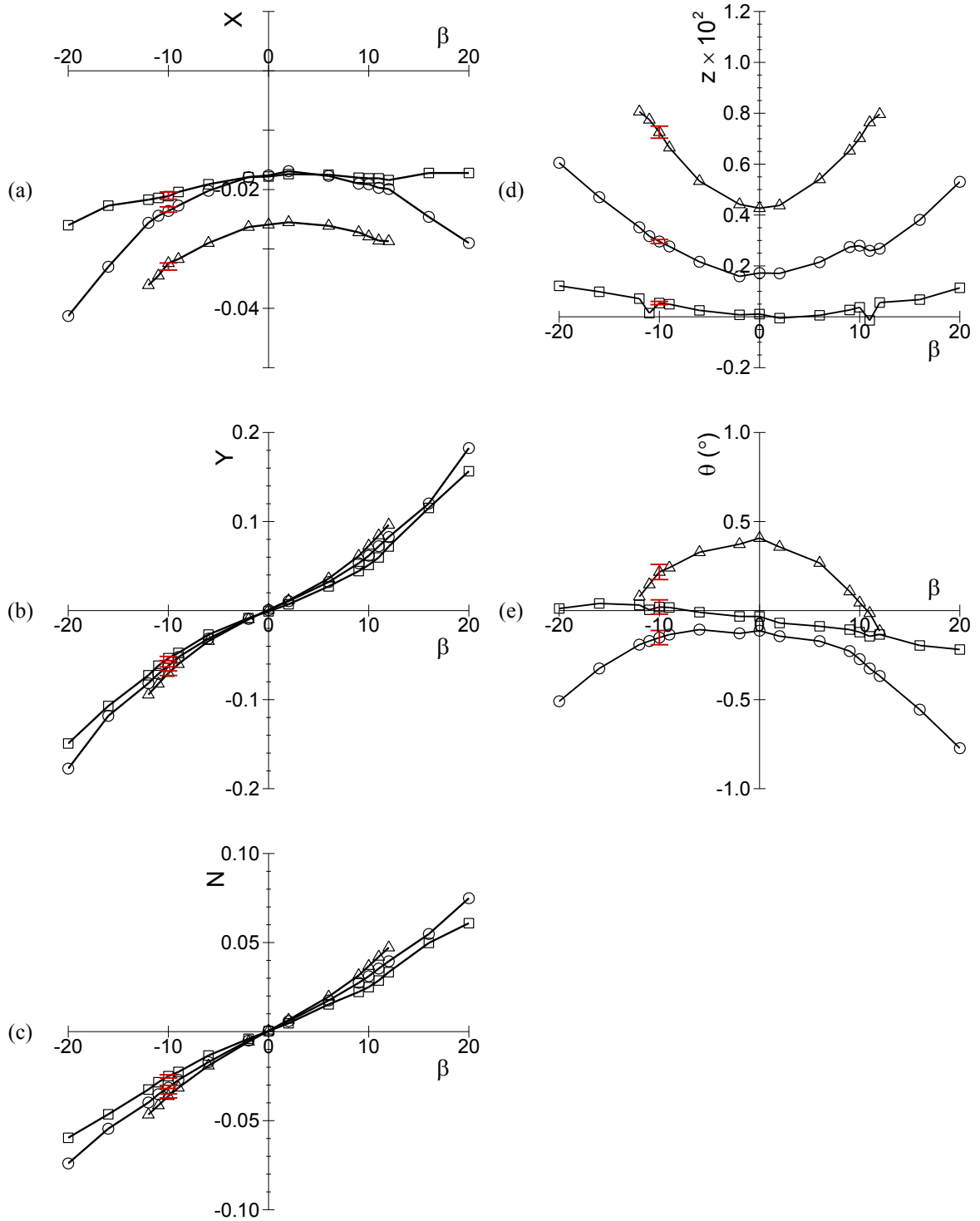
Figure 5-2 Static drift test results: (a) *X*; (b) *Y*; (c) *N*, (d) *z*, (e) *θ*, respectively. Symbols:
□ *Fr* = 0.138 **o** *Fr* = 0.280, Δ *Fr* = 0.410.
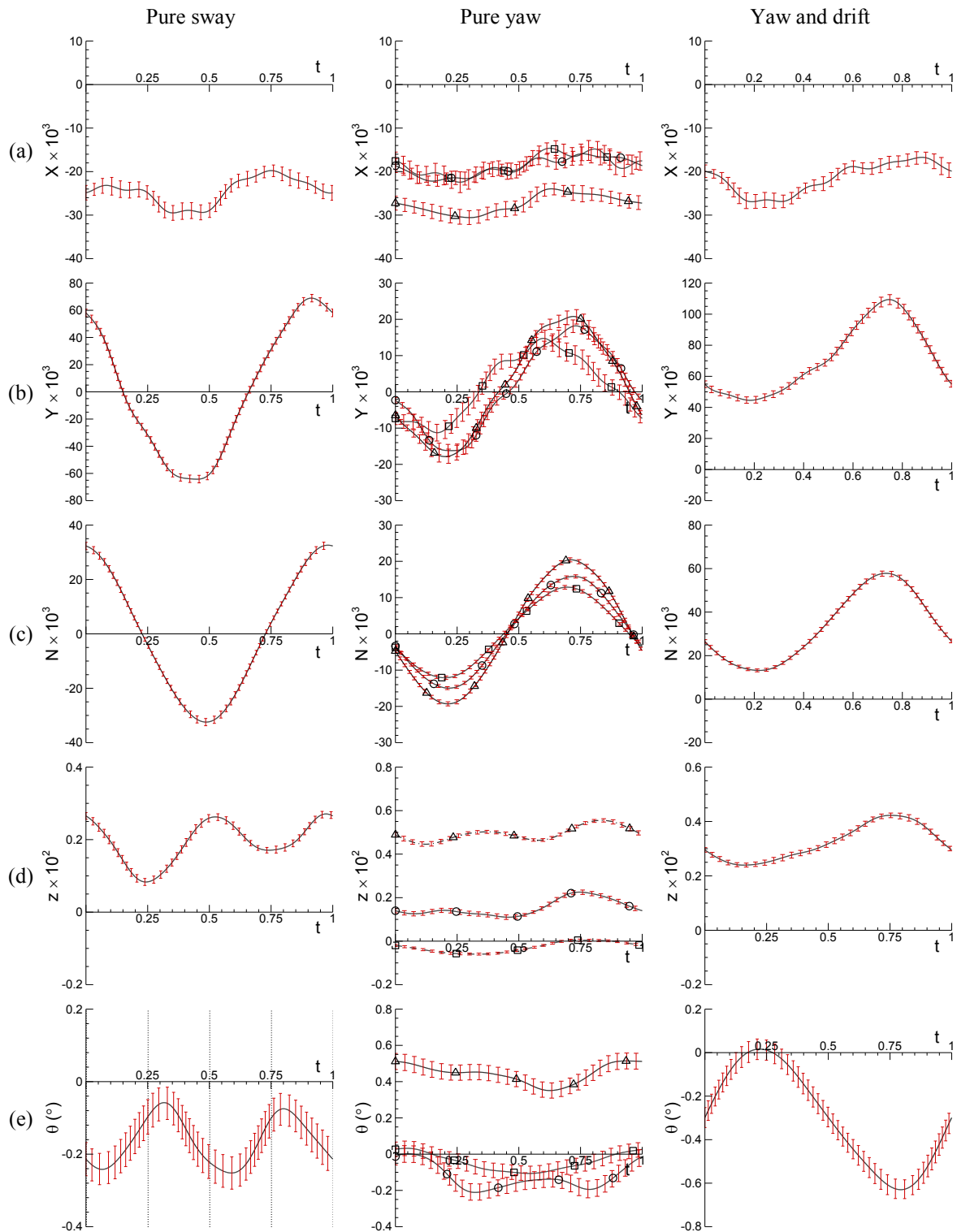
Figure 5-3 Dynamic test results: (a) *X*, (b) *Y*, (c) *N*, (d) *z*, and (e) *θ* for pure sway (left, β_{max} = 10°), pure yaw (center, r_{max} = 0.30), and yaw and drift (right, β = 10°) tests, respectively. Symbols for pure yaw data: □ *Fr* = 0.138 ○ *Fr* = 0.280, △ *Fr* = 0.410.
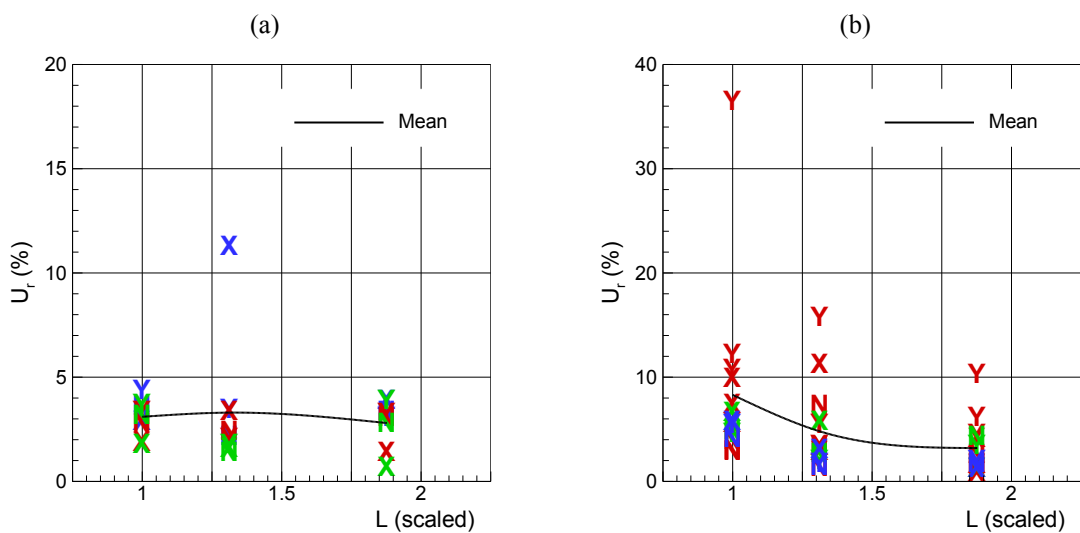
Figure 5-4 Comparisons of UA between facilities (Scale effect): (a) Static drift data (X,Y,N: Fr = 0.138; X,Y,N: Fr = 0.280; X,Y,N: Fr = 0.410) and (b) Dynamic tests data (X,Y,N: Pure sway; X,Y,N: Pure yaw; X,Y,N: Yaw and drift).
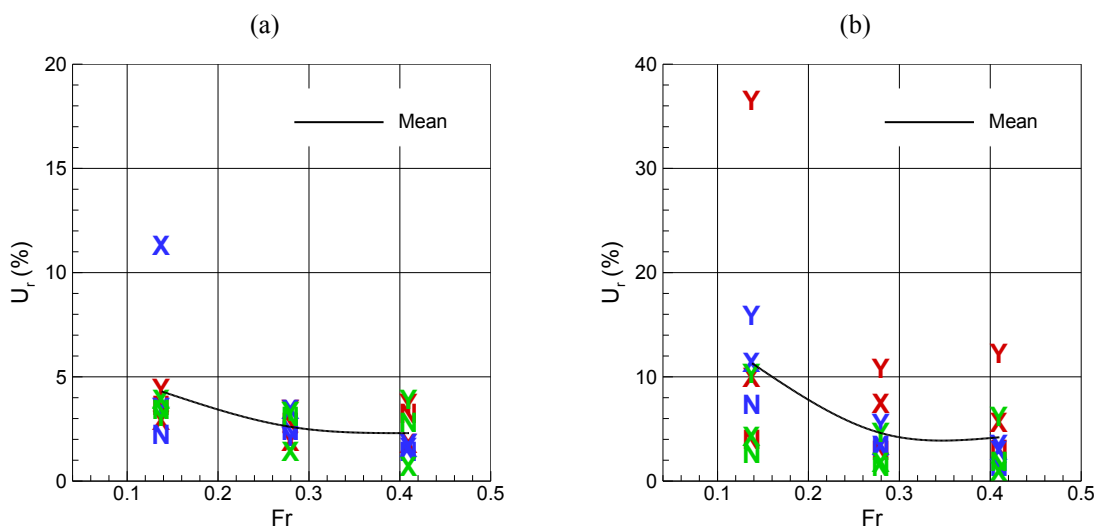
Figure 5-5 Comparisons of UA between facilities (Fr effect): (a) Static drift data and (b) Dynamic tests data. Symbols: X,Y,N, IIHR; X,Y,N, FORCE; X,Y,N, IN-SEAN.

5.2   UA for Phase-Averaged Flow Field

The uncertainty analysis (UA) of phase-averaged Stereo PIV measurement results follows the ASME PTC 19.1-2005 Standard (ASME 2005). The ASME (2005) is a revision of the ASME PTC 19.1-1998 Standard (ASME 1998) that is equivalent to the AIAA (1999) standard. The approach of ASME (1998)/AIAA (1999) is error/uncertainty definitions, systematic/random categorizations, and large sample size/normal distribution 95% level confidence interval assumptions. The details of the ASME (1998)/AIAA (1999) are derived and explained in Coleman and Steele (1995).

The main revision of the ASME (2005) from its previous version, ASME 1998, is focused on the harmonization with the ISO Guide (1995) that utilizes conceptually different error/uncertainty classifications (Type A and Type B) from the ASME (1998)/AIAA (1999). For this, the ASME 2005 adapts nomenclatures more consistent with the ISO Guide (1995): 1) the terms 'bias' and 'precision' are not used therein, however, uncertainties remain conceptualized as 'systematic' and 'random', respectively, and 2) the term 'standard' uncertainty is introduced and the terms such as 'combined standard' uncertainty and 'expanded' uncertainty are used instead of the term 'total' uncertainty.

5.2.1   UA Methodology (ASME 2005)

Measurement error, the difference between the measured value X and the true value, consists of two components: *random error* (ϵ) that varies randomly in repeated measurements and *systematic error* (β) that remains constant throughout the test. Measurement uncertainty is the combination of *random uncertainty* (s) due to the random error and *systematic uncertainty* (b) due to the systematic error.

Random error causes scatters in successive measurements of X from which sample mean $\bar{X}$ and sample standard deviation s_X are calculated. The random standard uncertainty of the sample mean, $s_{\bar{X}}$, then, can be used to define the probable interval containing

the population (true) mean of the measurement with a defined level of confidence, which is given as

$$s_{\bar{X}} = s_X / \sqrt{N} \tag{5.38}$$

where N is the number of repeat measurements. For a normal distribution and a large sample size ($N > 30$), for example, the interval $\bar{X} \pm 2s_{\bar{X}}$ is expected to contain the true mean with 95% confidence.

The measurement is influenced by several different elemental systematic error sources, each of which may be postulated to come from a population of possible error values. Systematic standard uncertainty of the measurement is a combination of the elemental systematic errors from all the error sources such that

$$b_{\bar{X}} = \left[\sum_{k=1}^{K} \left(b_{\bar{X}_k} \right)^2 \right]^{\frac{1}{2}} \tag{5.39}$$

where the elemental systematic standard uncertainty $b_{\bar{X}_k}$ represents the dispersion of possible elemental systematic error values $\beta_{\bar{X}_k}$ at the standard deviation level.

The elemental systematic standard uncertainties are usually evaluated from a) engineering judgment, b) published information, or c) special data. *Engineering judgment* is to use engineering analysis and experience to estimate an interval for elemental systematic error within which 95% of possible $\beta_{\bar{X}_k}$ values are expected. Typically $\beta_{\bar{X}_k}$ is assumed as normal distribution and spread symmetric (equally in both the positive and negative directions) with a large degree of freedom ($v \geq 30$). Subsequently the elemental systematic standard uncertainty is estimated as

$$b_{\bar{X}_k} = B_{\bar{X}_k} / 2 \tag{5.40}$$

where $B_{\bar{X}_k}$ represents the 95% confidence level estimate of the symmetric limits of error associated with the kth elemental error source. Next, the *published information* includes calibration reports, instrument specifications, and other technical references that may provide quantitative information regarding the elemental systematic errors, such as a confidence interval, an ISO expanded uncertainty statement, or a multiple of a standard deviation. In these cases, $b_{\bar{X}_k}$ is estimated by dividing those information values by the statistic value such as the Student's t, by the coverage factor (or the "k factor"), or by the multiplier, respectively. Lastly, the *special data* include inter-laboratory or inter-facility tests and comparisons of independent measurements that depend on different principles or that have been made by independently calibrated instruments (See Section 4-3.2.2.3 of ASME 2005).

For a calculated result R that is expressed as a function of measured (averaged) or assigned values of independent parameters (X_i) as

$$R = f(\bar{X}_1, \bar{X}_2, \dots, \bar{X}_I) \tag{5.41}$$

the uncertainties of those parameters may propagate to the result through the functional relationship. The error propagations can be approximated by a Taylor series method (See Nonmandatory Appendix C of ASME 2005), typically up to the first order, and the sensitivity (or sensitivity coefficient) θ_i of the parameter $\bar{X}_i$ is defined as

$$\theta_i = \frac{\partial R}{\partial \bar{X}_i} \tag{5.42}$$

of which partial differentiation can be evaluated either analytically or numerically. Then, the systematic standard uncertainty of R is determined from the propagation equation as

$$b_R = \left[\sum_{i=1}^{I} \left(\theta_i b_{\bar{X}_i} \right)^2 \right]^{\frac{1}{2}} \tag{5.43}$$

When more than one test is conducted with the same instrument package (i.e., repeated tests), the estimate of the standard deviation of the distribution of the results is

$$s_R = \left(\frac{\sum_{m=1}^{M}(R_m - \bar{R})^2}{M-1}\right)^{\frac{1}{2}} \tag{5.44}$$

where M is the number of tests, and the random standard uncertainty of the mean result $\bar{R}$ is

$$s_{\bar{R}} = s_R/\sqrt{M} \tag{5.45}$$

The root-sum-square of the systematic and random standard uncertainties is calculated to determine the 'combined' standard uncertainty of R as

$$u_R = [(b_R)^2 + (s_R)^2]^{\frac{1}{2}} \tag{5.46}$$

Finally, the combined standard uncertainty is expanded to the 95% level of confidence, termed as the 'expanded' uncertainty, by multiplying appropriate expansion factor t_{95} as

$$U_{R,95} = t_{95} \cdot u_R \tag{5.47}$$

where the expansion factor (or 'coverage factor') t_{95} value, with the degree of freedom ν_R known, is obtained from the Student t statistic at the 95% confidence level, and $t_{95} = 2$ for large degrees of freedom ($\nu_R \geq 30$). When the degree of freedom for one of the systematic and random standard uncertainties or for both is not large ($\nu_R < 30$), an effective degree of freedom may be obtained by using the Welch-Satterthwaite formula (Nonmandatory Appendix B of ASME 2005).

$$\nu_R = \frac{\left\{\sum_{i=1}^{I}[(\theta_i b_i)^2 + (\theta_i s_i)^2]\right\}^2}{\sum_{i=1}^{I}\left[\frac{(\theta_i s_i)^4}{\nu_{s_i}} + \sum_{k=1}^{K_i}\frac{(\theta_i b_{i_k})^4}{\nu_{b_{i_k}}}\right]} \tag{5.48}$$

where $\nu_{s_i} = N_i - 1$ is the degree of freedom of the random standard uncertainty s_i and $\nu_{b_{i_k}}$ is the degree of freedom of the kth elemental uncertainty of the systematic standard uncertainty b_i which can be approximated as

$$\nu_{b_{i_k}} = \frac{1}{2}\left(\frac{\Delta b_{i_k}}{b_{i_k}}\right)^{-2} \tag{5.49}$$

where the quantity in parentheses is an estimate of the relative variability of the estimate of b_{i_k} (See the ISO Guide 1995)

5.2.2 UA Procedures

The basic underlying idea of present UA procedures for the Stereo PIV (SPIV) measurement is to calibrate the SPIV measured data to the known reference values. An example can be a UA for a measurement of flow velocity V behind a model using a Pitot probe at a towing tank facility. The uncertainty in V may be estimated by using a data reduction equation such as $V = \sqrt{2\Delta p/\rho}$ from the Bernoulli's equation, along with considerations of the elemental uncertainties in the pressure difference Δp and water density ρ measurements. Alternatively, the Pitot measurement can be calibrated to a reference measurement data such as the towing carriage speed U_C data, with known uncertainty. If a calm and open (i.e. no model installed) water is measured with the Pitot probe towed at a certain carriage speed U_C, then, the difference between the V and U_C can be considered as the systematic (bias) uncertainty of the Pitot measurement, relative to the U_C measurement and uncertainty.

Similar UA approach is used herein for SPIV measurement. For this, undisturbed open water is measured with the SPIV that is undergoing a forced PMM motion. As no model is installed, SPIV measured data are the free stream flow data of which values can be determined as well from the PMM measured sway and yaw motion data by using the coordinate transformation relationship between the PMM- and PIV-fixed coordinate sys-

tems as shown in Section 3.1.2. Then, the PMM measured free stream data are used as the reference to be compared with the SPIV measurements estimating the systematic uncertainties.

The open water measurement includes two test cases: *Case 1) Uniform flow measurement* and *Case 2) Open water pure yaw test*. The former case is the simplest case where the calm and open water is measured as the PIV system is towed straight at a constant speed U_C with no PMM motions. For the latter case, the undisturbed open water is measured as the PIV system is undergoing a forced pure yaw PMM motions. Test conditions are summarized in Table 5-15 for both cases.

An overall schematic (flow chart) of the present UA procedure is shown in Fig. 5-6, where the procedures are grouped into three stages; designated as A, B, and C in the figure. A) The systematic standard uncertainties of the measurements are estimated and the sources of the possible elemental errors are identified. B) The PMM measured reference values are calculated and the phase-averaged PIV data from the open water tests are compared. The elemental measurement uncertainties from the previous stage are propagated through the data reduction process. C) The uncertainties in the test results such as the phase-averaged mean velocity, Reynolds stresses, turbulent kinetic energy, and the axial vorticity are estimated by combining the systematic and random standard uncertainties and then expanded to the 95% confidence level by multiplying a proper expansion factor.

5.2.2.1 Systematic standard uncertainty

The elemental systematic uncertainties of measurements include b_{U_C}, b_Y, b_ψ, b_{dx}, and b_{dy} in the measurements of carriage speed U_C, PMM sway displacement Y and yaw angle ψ, and field point location dx and dy, respectively. $b_{U_C} = B_{U_C}/2 = 0.005$ m/s, where the bias limit of carriage speed $B_{U_C} = 0.010$ m/s is from the carriage speed calibration as per Section 5.1.1. $b_Y = 0.05$ mm is from the sway potentiometer calibration. $b_\psi =$

$B_\beta/2 = 0.11°$, where the bias limit $B_\beta = 0.22°$ is from the drift angle calibration as per Section 5.1.1. $b_{dx} = b_{dy} = 0.5$ mm is from the tape measure accuracy for dx and dy measurements. These elemental systematic uncertainties propagate through the data reduction equations (DRE's) shown in Section 3.5.2, and are used to estimate the SPIV measurement results, i.e. the turbulent flow field data around the model in PMM motion, as follows.

Let result $R = U_i$, u_iu_j, k, and ω_x from the SPIV measurement. U_i is velocity components and $i = 1, 2, 3$ for U, V, W, respectively, and u_iu_j is Reynolds stress where i, $j = 1, 2, 3$ for uu, vv, ww, uv, uw, vw in combinations, and k is the turbulent kinetic energy, and ω_x is the axial vorticity. The systematic uncertainty is determined herein by comparing (or calibrating) the R with the corresponding reference data, R_{Ref}.

The overall procedure evaluating the systematic standard uncertainty of the results, b_R, is conceptually similar as typical measurement device calibration; the reference data R_{Ref} is used as the calibration standard and the difference that is defined as

$$\delta = R - R_{Ref} \tag{5.50}$$

is considered as the systematic or bias error of R with respect to R_{Ref}. If the standard limit of the systematic error, b_δ, and the systematic standard uncertainty of the reference data, $b_{R_{Ref}}$, are known, then, b_R is the root-sum-square of those elemental uncertainties, b_δ and $b_{R_{Ref}}$, as per the equation (5.39) such that

$$b_R = \left(b_\delta^2 + b_{R_{Ref}}^2\right)^{\frac{1}{2}} \tag{5.51}$$

where

$$b_\delta = \left[\bar{\delta}^2 + \left(2 \cdot \frac{s_\delta}{\sqrt{M}}\right)^2\right]^{\frac{1}{2}}/2 \tag{5.52}$$

$b_\delta = B_\delta/2$ as per (5.40), where B_δ, i.e. the numerator at the right hand side of (5.52), is the systematic limit of δ at the 95% confidence level by assuming a normal distribution of δ with a large degree of freedom ($M > 30$). $\bar{\delta}$ and s_δ in (5.52) are the mean and standard deviation of the δ values collected from a number M of repeat measurements, respectively. The other elemental systematic uncertainty of b_R in (5.51), $b_{R_{Ref}}$, is defined and evaluated in two different ways according to the result variable R as follows.

The R_{Ref} is from the free stream data, introduced at the later part of Section 3.1.2, measured from the aforementioned open water tests. Knowing that the free stream flow is only in the horizontal plane of the ship-fixed x-y coordinate system (Fig. 3-4), expected from the free stream flow are no velocity in the vertical direction, no turbulence in the flow, and no velocity gradient in the cross-flow plane. Accordingly, R_{Ref} data are not measured for $R = W$, $u_i u_j$, k, and ω_x from the open water tests, but the expected value is used as the reference, i.e. $R_{Ref} = 0$, thus $b_{R_{Ref}} = 0$.

For $R = U$ and V, on the other hand, R_{Ref} is using the longitudinal u_P and the lateral v_P velocities of the free stream in the ship-fixed coordinate system (Fig. 3-4), respectively. Let $R_{PMM} = u_P$ and v_P, then R_{Ref} is the normalized R_{PMM} with the carriage speed U_C such as

$$R_{Ref} = R_{PMM}/U_C \tag{5.53}$$

or $R_{Ref} = f(R_{PMM}, U_C)$ in a functional form. Then, the systematic standard uncertainty the reference data, $b_{R_{Ref}}$, is from the elemental systematic standard uncertainties, $b_{R_{PMM}}$ and b_{U_C}, propagated through the data reduction equation (DRE) (5.53) as

$$b_{R_{Ref}} = \left(\theta_{R_{PMM}}^2 b_{R_{PMM}}^2 + \theta_{U_C}^2 b_{U_C}^2\right)^{\frac{1}{2}} \tag{5.54}$$

as per the error propagation equation (5.43), where the sensitivity coefficients $\theta_{R_{PMM}} = \partial R_{Ref}/\partial R_{PMM}$ and $\theta_{U_C} = \partial R_{Ref}/\partial U_C$ are respectively as per (5.42).

The elemental systematic uncertainty $b_{R_{PMM}}$ of $R_{PMM} = f(U_C, V_P, r, \psi, dx, dy)$ as per the DRE's (3.5a) and (3.5b) in Section 3.1.3 (or in Section 3.5.2) for u_P and v_P, respectively, is from the further elemental systematic uncertainties, b_{U_C}, b_{V_P}, b_r, b_ψ, b_{dx}, and b_{dy}. The error propagation equation for $b_{R_{PMM}}$ can be written using (5.43) as

$$b_{R_{PMM}} = \left(\theta_{U_C}^2 b_{U_C}^2 + \theta_{V_P}^2 b_{V_P}^2 + \theta_r^2 b_r^2 + \theta_\psi^2 b_\psi^2 + \theta_{dx}^2 b_{dx}^2 + \theta_{dy}^2 b_{dy}^2\right)^{\frac{1}{2}} \tag{5.55}$$

Where the sensitivity coefficient $\theta_{X_i} = \partial R_{PMM}/\partial X_i$ for $X_i = U_C, V_P, r, \psi, dx,$ and dy is respectively as per (5.42).

Of the six elemental standard systematic uncertainties in (5.55), b_{V_P} is for $V_P = f(Y_0, \omega, \gamma)$ as per the DRE (3.23) and b_r is for $r = f(\psi_0, \omega, \gamma)$ as per the DRE (3.24), hence those uncertainties are even further elemental systematic standard uncertainties b_{Y_0}, b_{ψ_0}, b_ω, and b_γ, propagated through the DRE's. Y_0 and ψ_0 are the Fourier Series 1st-order harmonic amplitudes of the Y and ψ measurement data, respectively, thus any possible constant shift in Y and ψ, i.e. the systematic error, does not affect the Y_0 and ψ_0 values. Accordingly, b_Y and b_ψ do not propagate to Y_0 and ψ_0 through data reduction, and $b_{Y_0} = b_{\psi_0} = 0$. Next, b_ω is for $\omega = 2\pi(N/60)$, where N is the PMM frequency f_{PMM} in RPM. Then, $b_\omega = \left(\frac{2\pi \cdot B_N}{60}\right)/2 = 0.00003$ Hz, where $B_N = 0.0006$ rpm is the bias limit of N from Table 9 for PMM UA in Section 5.1.2. For IIHR PMM, b_ω is negligibly small such that $b_\omega/\omega = 0.0002$ for $\omega = 0.842$ (corresponding to $f_{PMM} = 0.134$ Hz), it can be assumed that $b_\omega = 0$. Consequently, b_{V_P} and b_r are from b_γ only, and their error propagation equations are written as

$$b_{V_P} = \left(\theta_\gamma^2 b_\gamma^2\right)^{\frac{1}{2}} \tag{5.56}$$

$$b_r = \left(\theta_\gamma^2 b_\gamma^2\right)^{\frac{1}{2}} \tag{5.57}$$

where the sensitivity coefficient $\theta_\gamma = \partial V_P / \partial \gamma$ in (5.56) and $\theta_\gamma = \partial r / \partial \gamma$ in (5.57), respectively. b_γ in (5.56) and (5.57) is for $\gamma = f(Y, \psi, Y_0, \psi_0)$ as per DRE (3.27) in Section 3.5.2, and from the elemental systematic uncertainties b_Y, b_ψ, b_{Y_0}, and b_{ψ_0}, where $b_{Y_0} = b_{\psi_0} = 0$ as previously discussed. Then, the error propagation equation for b_γ can be written as

$$b_\gamma = \left(\theta_Y^2 b_Y^2 + \theta_\psi^2 b_\psi^2 \right)^{\frac{1}{2}} \tag{5.58}$$

where the sensitivity coefficients $\theta_Y = \partial \gamma / \partial Y$ and $\theta_\psi = \partial \gamma / \partial \psi$, respectively as per (5.42).

5.2.2.2 Random standard uncertainty

The random standard uncertainty s_R of the previously defined result R is estimated by performing 'end-to-end' multiple tests at the same test conditions. Herein the term 'end-to-end' implies that the whole data acquisition/reduction procedures described in Sections 3.7.2/3.8.2 are repeated to see the overall scatters in the results as a consequence of all possible elemental random errors. For the multiple tests, the location of the PIV system relative to the ship model was perturbed each time of the multiple tests by repositioning the PIV system in the (x, y, z) directions. Note, however, that the same towing tank facilities, the same PMM, the same model, the same PIV system including its calibration are used for the multiple tests due to limited experimental resources.

Total three sets ($M = 3$) of test are performed; each test consists of more than 100 carriages runs for the phase averaging purposes. Each carriage run is made with about 12-minute interval between the runs to minimize flow disturbances from previous runs. Each test set takes typically one day for test setup and 3 ~ 4 days for data acquisition, thus spanning total 4 ~ 5 days. The mean result $\bar{R}$ is calculated from the results of mul-

tiple tests, used to calculate the random standard uncertainty s_R using the equation (5.38) with $M = 3$.

5.2.2.3   Combined standard and expanded uncertainty

Combined standard uncertainty u_R of the result is the root-sum-square of the systematic standard uncertainty b_R and the random standard uncertainty s_R as per the equation (5.46) in Section 5.2.1. The systematic uncertainty b_R is from (5.51) and the random standard uncertainty s_R is using the equation the equation (5.38) from the multiple tests.

Expanded uncertainty $U_{R,95}$ of the result is as per the equation (5.47) in Section 5.2.1. The expansion factor t_{95} in (5.47) is estimated using the Welch-Satterthwaite formula shown in (5.48) as the degree of freedom of the random standard uncertainty estimation, $\nu_{s_R} = M - 1 = 2$, is smaller than 30 for the large sample assumption. The Welch-Satterthwaite formula (5.48) can be rewritten for the present UA as

$$\nu_R = \frac{\left\{(b_R)^2 + (s_R)^2\right\}^2}{(b_R)^4/\nu_{b_R} + (s_R)^4/\nu_{s_R}} \tag{5.59}$$

5.2.3   UA Results and Discussions

5.2.3.1   Open water Tests

Case 1) Uniform flow measurement:

The SPIV measurement area is located at 51 mm off from the towing tank centerline and at 93 mm below the calm water free surface line. A total 12 repeat tests are made, where the average towing carriage speed $\overline{U_C} = 1.5232$ m/s with a standard deviation of 0.0028 m/s (0.2% of $\overline{U_C}$). Each test is a single carriage run with 94 data samples acquired at a rate of 5 Hz ($\Delta t = 200$ ms) and reduced as per Section 3.5.2. Note that the data reduction in this case is not a phase-average but a time-average of the 94 data as no phase information.

In Fig. 5-7, test result R (shown as colored contours) and the systematic standard uncertainty b_R (labeled line contours) are shown for (a) U, (b) V, (c) W, (d) uu, (e) vv, (f) ww, (g) uv, (h) uw, (i) vw, (j) k, and (l) ω_x, respectively. R is the mean value of each variable data from the 12 repeat test, non-dimensional with U_C for U, V, W, with U_C^2 for uu, vv, ww, uv, uw, vw, and k, and with U_C/L for ω_x, respectively, where $L = 3.048$ m is the model length. b_R is evaluated as per Section 5.2.2.1 and presented as non-dimensional similarly as for R. The evaluation of b_R is summarized in Table 5-17 including the elemental uncertainties used in Section 5.2.2.1. All the data in the table are the spatially averaged values of those over the SPIV measurement area.

From Fig. 5-7 (a) – (c), velocities in general $U = 0.98 \sim 1.0$, $V = 0.01 \sim 0.02$, $W = -0.01 \sim 0.01$, respectively, of which mean difference (from the 12 repeat tests) from the reference value ($R_{Ref} = 1.0, 0.0, 0.0$, respectively) $\bar{\delta} = -0.0062, 0.0150, -0.0004$ in average, respectively. $b_U = 0.004 \sim 0.007$, $b_V = 0.004 \sim 0.012$, $b_W = 0 \sim 0.003$, corresponding respectively to about 0.6%, 0.8%, and 0.1% of U_C in average. b_U is the root-sum-square (RSS) of b_δ and $b_{R_{Ref}}$ as per (51), where $b_{R_{ref}} = \left(2 \cdot b_{U_C}^2 / U_C^2\right)^{\frac{1}{2}} = 0.0046$ from (54) by using $R_{PMM} = U_C$, and $b_{U_C} = 0.005$ m/s from Table 5-16. Whereas, b_V and b_W are the same as b_δ of V and W, respectively, as $b_{R_{Ref}} = 0$ for both. The evaluations of b_δ for U, V, W are as per (52), summarized in Table 5-17.

From Fig. 5-7 (d) – (f), the normal Reynolds stresses in general $uu = 0.0001 \sim 0.0004$, $vv = 0.0001 \sim 0.0003$, and $ww = 0 \sim 0.0001$, corresponding to $\sqrt{uu} = 1.6\%$, $\sqrt{vv} = 1.4\%$, $\sqrt{ww} = 0.8\%$ of U_C, respectively, in average. Shear stresses, from Fig. 5-7 (g) – (i), are in general $uv = 0.0001 \sim 0.0003$, $uw = -0.00003 \sim 0.00004$, and $vw = -0.00004 \sim 0.00004$, corresponding to $\sqrt{uv} = 1.3\%$ of U_C and $\sqrt{uw} \approx \sqrt{vw} \approx 0$ in average. Turbulent kinetic energy k shown in Fig. 5-7 (j) is similar with uu. The systematic standard uncertainty is as per (51) using (52) and $b_{R_{Ref}} = 0$ for those variables; $b_{uu} = 0.00013$, $b_{vv} = 0.00010$, $b_{ww} = 0.00003$ for the normal stresses, $b_{uv} = 0.00009$, $b_{uw} = 0.00001$, $b_{vw} =$

0.00001 for shear stresses, and b_k = 0.00013 for turbulent kinetic energy, respectively, summarized in Table 5-17.

From Fig. 5-7 (k), the axial vorticity is in general ω_x = -3 ~ 3 except for the region at the right side where locally strong ω_x = -8 ~ 7 exhibiting a particular cascade-shaped pattern. This pattern will be discussed below. b_{ω_x} = 1.2 in average, evaluated as per (51) using (52) and $b_{R_{Ref}}$ = 0, summarized in Table 5-17.

Possible sources of the systematic uncertainty of SPIV measurement may include the intrusive disturbance effect of the SPIV system. The displacement effect of the SPIV system is measured with a one-hole Pitot probe and the result is shown in Fig. 5-8. The axial velocity U of the free stream is measured along the longitudinal axis x through the center point of the SPIV measurement area, at several locations between x/D = -5 ~ 10, where D = 100 mm is the diameter of the SPIV camera housings (See Fig. 3-10) and x = 0 is located at the measurement area center point. Measurement result reveals the retarded flow around the camera housings, at maximum U/U_C = 0.9585 near at x/D = -4, due to the displacement effect. At x/D = 0, the measurement area location, the retarded velocity U/U_C = 0.9937 or the amount of retardation 1 - U/U_C = 0.0063, which are comparable with $\bar{\delta}$ = 0.9938 and b_U = 0.0058 of the uniform flow U measurement shown at Table 5-17. The error bars shown at x/D = 0 in Fig. 5-8 depict the $\pm 2 \cdot s$ range, where s = 0.0011 is the standard deviation of U/U_C values from five repeated measurements.

Another possible source of the systematic uncertainty may be the SPIV evaluation error such as the registration error (Scarano et al. 2005, Coudert & Schon 2001, Prasad 2000, Willert 1997, Prasad & Adrian 1993). The registration error is due to the mismatched SPIV image pairs in the interrogation process, which produces a particular pattern so called Moiré pattern in the dewarped PIV images. The Moiré pattern can be seen from Fig. 5-7 (a) – (c) and (k) for U, V, W, and ω_x, the cascade-shaped pattern at the right side of the measurement area. The Moiré pattern is more distinct for V which results in the rather strong Moiré pattern of ω_x through the data reduction process.

Case 2) Open water pure yaw test:

A total three tests are conducted with designated as Test 1, 2, and 3 respectively. SPIV measurements are at two different longitudinal positions $x/L = 0.935$ for Tests 1 and 2 and $x/L = 0.002$ for Test 3, respectively, where $L = 3.048$ m is the model length. The vertical location is at $z/T = 1.1$ for Test 1 and Test 3 and $z/T = 0.5$ for Test 2, respectively, where $T = 0.136$ m is the model draft. The lateral position $y = 0$ for all tests. Where, the locations correspond to the center-point position of the SPIV measurement area in the Ship-fixed coordinate system (Fig. 3-4).

Test conditions are same for all tests, summarized in Table 5-15. A total 100 carriage runs are made for each test. The mean and standard deviation values of carriage speed U_C and PMM sway Y_0 and yaw ψ_0 amplitudes are summarized in Table 5-18 for Test 1. Sway Y and yaw ψ data are phase-sorted into 32 phase groups where the typical number of data is about $270 \sim 280$. Phase averaged Y and ψ values are summarized in Table5-19 for Test 1 and for selective phase groups (every $45°$ nominal phase angle), where the subsequent phase γ values calculated from the Y, ψ, Y_0, and ψ_0 data by using (3.27) in Section 3.5.2. are as well presented.

Test results are shown in Fig. 5-9. Presented in the figure are the difference $\delta = R - R_{Ref}$ defined at (5.50). The results $R = (U, V, W)$ is the SPIV measured flow velocity and the reference data $R_{Ref} = (u_P, v_P, 0)$, where u_P and v_P are respectively as per (3.5a) and (3.5b) in Section 3.5.2 using the PMM measured data. Each symbol in the figure represents the spatially averaged δ value over the SPIV measurement area, measured at each phase angle γ of each test. In general δ is function γ; δ is relatively larger between $\gamma = 180° \sim 360°$ for U and between $\gamma = 90° \sim 270°$ for V, whereas almost flat for W, respectively. δ may be a function of SPIV locations as well. For V (green colored), δ for Test 3 (symbol O; at $x/L = 0.002$) is rather different from those for Tests 1 and 2 (respectively symbols □ and Δ; at $x/L = 0.935$). For W (blue colored), δ for Test 1 (symbol □

and Δ; at $z/T = 1.1$) is larger than those for Test 2 (symbol Δ; at $z/T = 0.5$). Whereas for U (red colored), δ is almost same between the tests.

The evaluation of b_R is summarized in Table 5-20 for all variables. All the data values in the table are first averaged spatially over the SPIV measurement area and then for all phase positions. For velocity data, $b_U = 0.0078$, $b_V = 0.0068$, and $b_W = 0.0055$, corresponding to about 0.8%, 0.7% and 0.6% of U_C, respectively, and about 130%, 90%, and 390% of those from the uniform flow test, respectively. For Reynolds normal stresses, $b_{uu} = 0.00020$, $b_{vv} = 0.00011$, and $b_{ww} = 0.00004$, of which square-root values are corresponding to about 1.4%, 1.0%, and 0.6% of U_C, respectively. For shear Reynolds stresses, $b_{uv} = 0.00011$, $b_{uw} = 0.00001$, and $b_{vw} = 0.00001$, of which square-root values are corresponding to about 1.0%, 0.3%, and 0.3% of U_C, respectively. For turbulent kinetic energy, $b_k = 0.00017$ and $\sqrt{2/3 \cdot b_k} = 1.1\%$ of U_C. b_{uu} and b_k are 154% and 131% of those from the uniform flow test, whereas similar for other stress components. For axial vorticity $b_{\omega_x} = 1.2$ is same as the uniform flow result.

5.2.3.2 Pure yaw test

Test is with model and as per the test conditions shown in Table 5-15, which are the same as those for open water pure yaw tests. The longitudinal location of the SPIV measurement is at $x/L = 0.135$. Test is more than 100 carriage runs allowing about 270 ~ 280 data per each of 32 PMM phase positions for phase averaging. The whole test procedures are repeated for three times.

UA is estimating the systematic b_R and random s_R standard uncertainties to ascertain the combined standard uncertainty u_R as per (5.46). b_R is from the open water pure yaw test and s_R is from the three repeat tests as per (5.45) using $M = 3$. u_R is used to estimate the expanded uncertainty $U_{R,95}$ as per (5.47) where the expansion factor $t_{95} = 2.365$ corresponding to the Student t statistic for a degree of freedom $v_R = 7$ and for a 95% confidence level. v_R is estimated by using (5.59) as per the Welch-Satterthwaite

formula (5.48), where for (5.59), $v_{b_R} = 8$ is used as per (5.49) for $b_{i_k} = b_R$ by assuming the relative variability of the estimate $\Delta b_R / b_R = 0.25$ as per the example case (B-1.10) in Appendix B of ASME (2005).

Pure yaw test result R and the relative expanded uncertainty $U_{R,95}$ (% R) is shown in Fig. 5-10 for (a) U, (b) V, (c) W, (d) uu, (e) vv, (f) ww, (g) uv, (h) uw, (i) vw, (j) k, and (k) ω_x at the PMM phase $\gamma = 236.25°$ position, respectively. The results shown in the figure are the mean values of the three repeat tests data. The center point position of the SPIV measurement area is located at $y/L = -0.0125$ laterally and at $z/L = 0.0525$ ($z/T = 1.1765$) vertically, respectively. The measurement area is split into two sub regions as shown in Fig. 5-10 (l) using $K = 0.45$ as a criteria, where $K = \frac{1}{2}(U^2 + V^2 + W^2)$ is the kinematic energy of the fluid. The Inner Region is where $K \leq 0.45$ representing the boundary layer region and the Outer Region is where $K > 0.45$ representing the free stream region of the flow, respectively. All the result values and the UA data value are averaged within the two regions respectively, and summarized in Tables 5-21 and 5-22 for the Inner and Outer region, respectively.

In the Inner Region, the random uncertainty is predominant, 60% ~ 99%, over the systematic uncertainty, 1% ~ 40%, for all variables except for V and W. For V and W, systematic uncertainty is dominant, 69% and 63%, respectively. The expanded uncertainty $U_{R,95} = 0.0321, 0.0213, 0.0188$ for U, V, W, respectively, corresponding to about 3.2%, 2.1%, and 1.9% of U_C, respectively, and to 3.9%, 29.1%, and 32.1% of the mean U, V, W values, respectively. For the normal Reynolds stresses, $U_{R,95} = 0.0014, 0.0007, 0.0003$ for uu, vv, ww, respectively, of which squqre-root value corresponds to about 4%, 3%, and 2% of U_C, respectively. For the shear Reynolds stresses, $U_{R95} = 0.0008, 0.0003, 0.0002$ for uv, uw, vw, respectively, of which square-root value corresponds to about 3%, 2%, and 1% of U_C, respectively. The relative uncertainties of the Reynolds stresses are 24% ~ 33% and 45% ~ 78% of the mean result values for the normal and shear stresses, respectively. For turbulent kinetic energy k, $U_{R,95} = 0.0011$ and

$\sqrt{2/3 \cdot U_{R,95}} = 2.7\%\ U_C$, and its relative uncertainty is 25% of the mean k value. For axial vorticity ω_x, $U_{R,95} = 15.2$ and the relative uncertainty is 36% of the mean ω_x value.

In the Outer Region, the systematic uncertainty is predominant, in general 70% ~ 96%, over the random uncertainty, in general 4% ~ 30%, for all variables except for ω_x. For ω_x, both systematic and random uncertainties are equally large, 52% and 48%, respectively. The expanded uncertainty $U_{R,95}$'s of U, V, W are relatively smaller than those for the Inner Region; about 2.4%, 1.5%, and 1.4% of U_C, respectively, or 2.5%, 12.1%, and 26.1% of the mean values, respectively. $U_{R,95}$ for the Reynolds stresses and the turbulent kinetic energy are also smaller than those for the Inner Region, about 0 ~ 0.0005, of which square-values are about 0 ~ 2% of U_C. However, the relative $U_{R,95}$ values are large, about 100% ~ 200%, due to very small mean values of those variables in the Outer Region. For axial vorticity ω_x, $U_{R,95} = 4.0$ and the relative uncertainty is large about 140% as well due to smaller mean value of ω_x in the Outer Region.

Consequently, the absolute uncertainty of the SPIV measurement is about 2 ~ 3% of U_C for the out of plane velocity component, U, and about 1 ~ 2% of U_C for the in-plane velocity components, V and W, respectively. The relative uncertainty is about 3 ~ 4%, 12 ~ 29%, and 26 ~ 32% for U, V, W, respectively. The relative uncertainties of U are comparable with the 2.4% of Gui et al. (2001a) and the 1.6% and 1.0 ~ 3.5% of Longo et al. (2007) for steady- and unsteady-flow, respectively. Whereas, the relative uncertainties of V and W are larger than the 4 ~ 8% of Gui et al. (2001a) and the 3 ~ 4% of Longo el al. (2007). Gui et al. (2001a) and Longo et al. (2007) are 2D-PIV measurements using the same IIHR towing tank facility and the same DTMB 5512 model as the present study, respectively. Note that the uncertainties of Gui et al. (2001a) and Longo et al. (2007) are relative to the dynamic ranges of measurements. The relative uncertainties of the Reynolds stresses, about 25% ~ 50% in general at the Inner Region, are larger than the 4 ~ 6% of Gui et al. (2001a) and the 3 ~ 6% of Longo et al. (2007) for steady flow, whereas those are comparable with the 10 ~ 45% of Longo et al. (2007) for unsteady flow. For

the SPIV measurement, the large random uncertainty in the Inner Region may be reduced by increasing the number of PIV images for the phase averaging. On the other hand, the large systematic uncertainty in the Outer Region can be improved by using more sophisticated SPIV algorithm to reduce the SPIV evaluation errors such as the registration error and by using more careful reference data to reduce the calibration errors.

Table 5-15 Open water tests conditions for Stereo PIV UA.

Test Case	Test description	U_C (m/s)	Y_0 (mm)	ψ_0 (°)	f (Hz)	Δt (ms)	$\Delta\gamma$ (°)	Number of data per run L	Number of runs per test K	Number of repeat tests M
Case 1)	Uniform flow	1.531	0.0	0.0	0.0	200.0	-	94	1	12
Case 2)	Open water pure yaw	1.531	326.1	10.2	0.134	233.2	11.25	88	100	3

- : Not applicable

Table 5-16 Elemental systematic standard uncertainties of the SPIV measurements.

Measurement variable X	Description	Unit	Symbol	Systematic standard uncertainty $b_{\bar{X}}$
U_C	Carriage speed	m/s	b_{U_C}	0.005
Y	Sway displacement	mm	b_Y	0.05
ψ	Yaw angle	deg	b_ψ	0.11
dx, dy	Field point location from the midship point	mm	b_{dx}, b_{dy}	0.5

Table 5-17 Systematic uncertainties of SPIV uniform flow measurement[†].

Result variable R	Average SPIV data $\bar{R}$	Reference data R_{Ref}	Average difference $\bar{\delta}$	Standard deviation of difference s_δ	Systematic standard uncertainty of difference b_δ	Systematic standard uncertainty of reference $b_{R_{Ref}}$	Systematic standard uncertainty of Result b_R
U	0.9938	1.0	-0.0062	0.0047	0.0034	0.0046	0.0058
V	0.0150	0.0	0.0150	0.0017	0.0075	0.0	0.0075
W	-0.0004	0.0	-0.0004	0.0008	0.0014	0.0	0.0014
uu	0.00025	0.0	0.00025	0.00006	0.00013	0.0	0.00013
vv	0.00019	0.0	0.00019	0.00004	0.00010	0.0	0.00010
ww	0.00006	0.0	0.00006	0.00002	0.00003	0.0	0.00003
uv	0.00017	0.0	0.00017	0.00004	0.00009	0.0	0.00009
uw	0.00000	0.0	0.00000	0.00002	0.00001	0.0	0.00001
vw	0.00000	0.0	0.00000	0.00002	0.00001	0.0	0.00001
k	0.00025	0.0	0.00025	0.00005	0.00013	0.0	0.00013
ω_x	-0.17	0.0	-0.17	2.2	1.2	0.0	1.2

† Presented varles are non-dimensional and averaged over the measurement area.

Table 5-18 Measurement data of U_C, Y_0, and ψ_0†.

Measurement variable			Mean value	Standard deviation
X	Unit	Nominal value	$\bar{X}$	s_X
U_C	m/s	1.531	1.5307	0.0059
Y_0	mm	326.1	328.42	0.0241
ψ_0	deg.	10.2	10.40	0.0566

† From open water pure yaw test with $N = 100$ carriage runs

Table 5-19 Measurement data of Y, ψ, and γ†.

		Y (mm)			ψ (°)			γ (°)	
Phase Group	Number of data	Nominal	Mean value	Standard deviation	Nominal	Mean value	Standard deviation	Nominal	Measured
n	N	value	$\bar{X}$	s_X	value	$\bar{X}$	s_X	value	value
1	276	0.0	0.7	1.6	-10.20	-10.33	0.05	0.0	-0.1
5	274	-230.6	-232.5	1.3	-7.21	-7.40	0.04	45.0	44.9
9	274	-326.1	-329.2	0.6	0.00	-0.06	0.04	90.0	89.7
13	278	-230.6	-234.4	0.4	7.21	7.35	0.05	135.0	134.7
17	273	0.0	-2.1	0.6	10.20	10.39	0.06	180.0	179.6
21	267	230.6	230.1	0.4	7.21	7.49	0.05	225.0	224.2
25	276	326.1	327.4	0.7	0.00	0.17	0.04	270.0	269.1
29	282	230.6	232.0	1.3	-7.21	-7.30	0.05	315.0	314.8

† From open water pure yaw test with $N = 100$ carriage runs.

Table 5-20 Summary of UA for open water pure yaw test ($M = 3$ repeat tests)†.

Result variable	Average difference	Standard deviation of differ-ence	Systematic standard uncertainty of differ-ence	Systematic standard uncertainty of refer-ence	Systematic standard uncertainty of Result
R	$\bar{\delta}$	s_δ	b_δ	$b_{R_{Ref}}$	b_R
U	-0.0111	0.0031	0.0060	0.0046	0.0078
V	0.0085	0.0064	0.0064	0.0024	0.0068
W	-0.0090	0.0055	0.0055	0.0	0.0055
uu	0.00038	0.00009	0.00020	0.0	0.00020
vv	0.00021	0.00005	0.00011	0.0	0.00011
ww	0.00007	0.00002	0.00004	0.0	0.00004
uv	0.00022	0.00005	0.00011	0.0	0.00011
uw	0.00000	0.00002	0.00001	0.0	0.00001
vw	0.00000	0.00001	0.00001	0.0	0.00001
k	0.00033	0.00006	0.00017	0.0	0.00017
ω_x	-0.1	1.7	1.2	0.0	1.2

Table 5-21 Summary of UA for pure yaw test with model (Inner Region).

Result variable	Result	Systematic standard uncertainty	Random standard uncertainty	Combined standard uncertainty	Relative systematic uncertainty contribution	Relative random uncertainty contribution	Expanded uncertainty	Relative expanded uncertainty
	R	b_R	s_R	u_R	b_R^2/u_R^2 (%)	s_R^2/u_R^2 (%)	U_{95R}	U_{95R}/R (%)
U	0.8326	0.0081	0.0101	0.0136	39.4	60.6	0.0321	3.9
V	0.0733	0.0071	0.0048	0.0090	68.6	31.4	0.0213	29.1
W	0.0586	0.0059	0.0045	0.0079	63.2	36.8	0.0188	32.1
uu	0.0044	0.0002	0.0005	0.0006	12.0	88.0	0.0014	32.9
vv	0.0026	0.0001	0.0003	0.0003	13.6	86.4	0.0007	26.2
ww	0.0014	0.0000	0.0001	0.0001	7.4	92.6	0.0003	24.0
uv	0.0017	0.0001	0.0003	0.0003	13.1	86.9	0.0008	45.3
uw	0.0004	0.0000	0.0001	0.0001	0.8	99.2	0.0003	74.0
vw	0.0003	0.0000	0.0001	0.0001	0.9	99.1	0.0002	77.8
k	0.0042	0.0002	0.0004	0.0004	16.3	83.7	0.0011	24.9
ω_x	41.8	1.7	6.0	6.4	7.2	92.8	15.2	36.3

Table 5-22 Summary of UA for pure yaw test with model (Outer Region).

| Result variable	Result	Systematic standard uncertainty	Random standard uncertainty	Combined standard uncertainty	Relative systematic uncertainty contribution	Relative random uncertainty contribution	Expanded uncertainty	Relative expanded uncertainty
	R	b_R	s_R	u_R	b_R^2/u_R^2 (%)	s_R^2/u_R^2 (%)	U_{95R}	U_{95R}/R (%)
U	0.9772	0.0098	0.0020	0.0102	95.9	4.1	0.0240	2.5
V	0.1236	0.0060	0.0015	0.0063	93.9	6.1	0.0149	12.1
W	0.0536	0.0057	0.0012	0.0059	95.9	4.1	0.0140	26.1
uu	0.0004	0.0002	0.0000	0.0002	94.7	5.3	0.0005	128.3
vv	0.0002	0.0001	0.0000	0.0001	95.1	4.9	0.0003	116.2
ww	0.0001	0.0000	0.0000	0.0000	92.6	7.4	0.0001	105.9
uv	0.0002	0.0001	0.0000	0.0001	95.7	4.3	0.0003	141.3
uw	0.0000	0.0000	0.0000	0.0000	72.5	27.5	0.0000	178.0
vw	0.0000	0.0000	0.0000	0.0000	77.1	22.9	0.0000	212.8
k	0.0004	0.0002	0.0000	0.0002	95.8	4.2	0.0004	118.7
ω_x	2.9	1.1	1.1	1.7	51.7	48.3	4.0	141.4
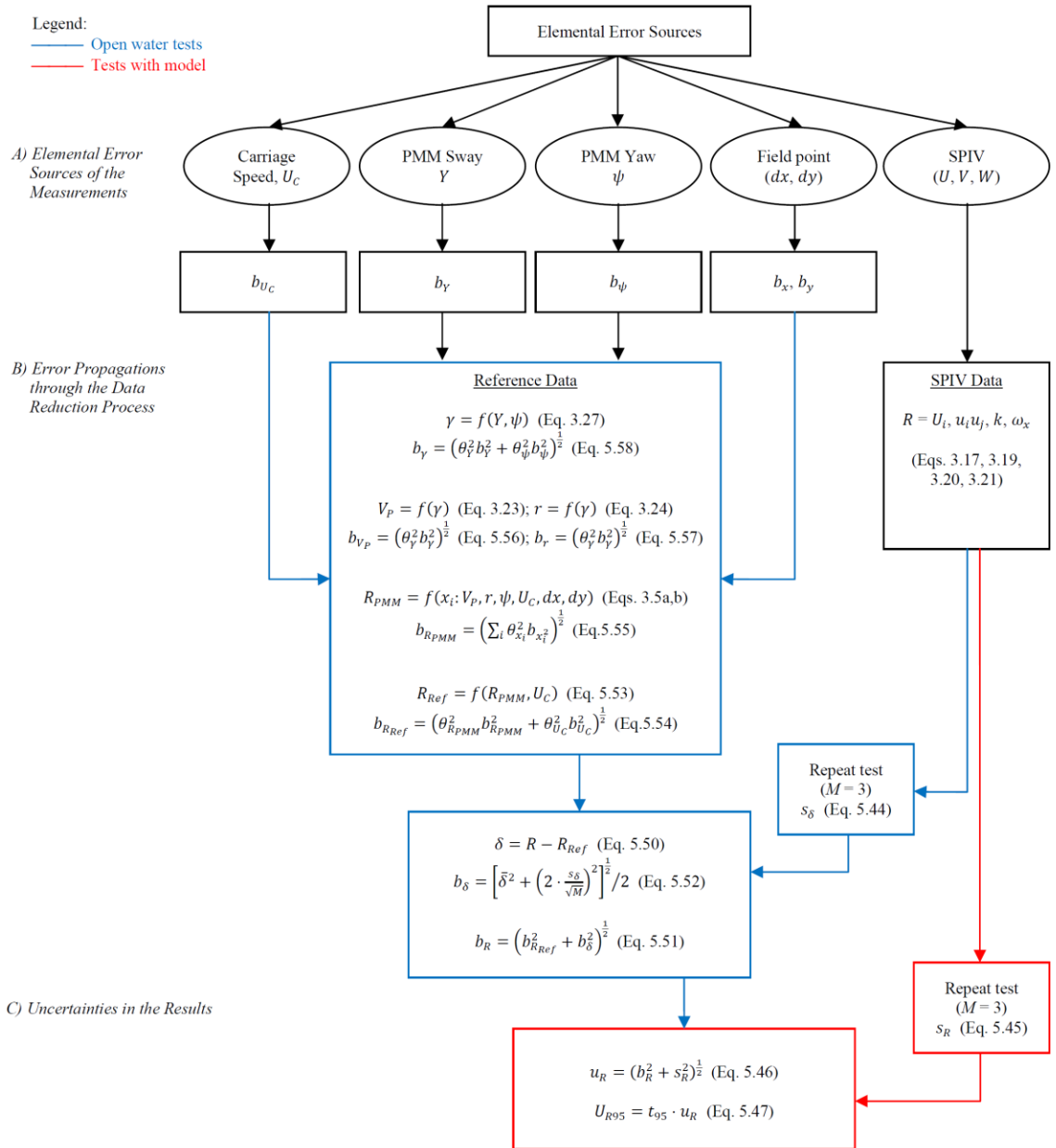
Figure 5-6 Error propagation chart for SPIV measured flow field data.
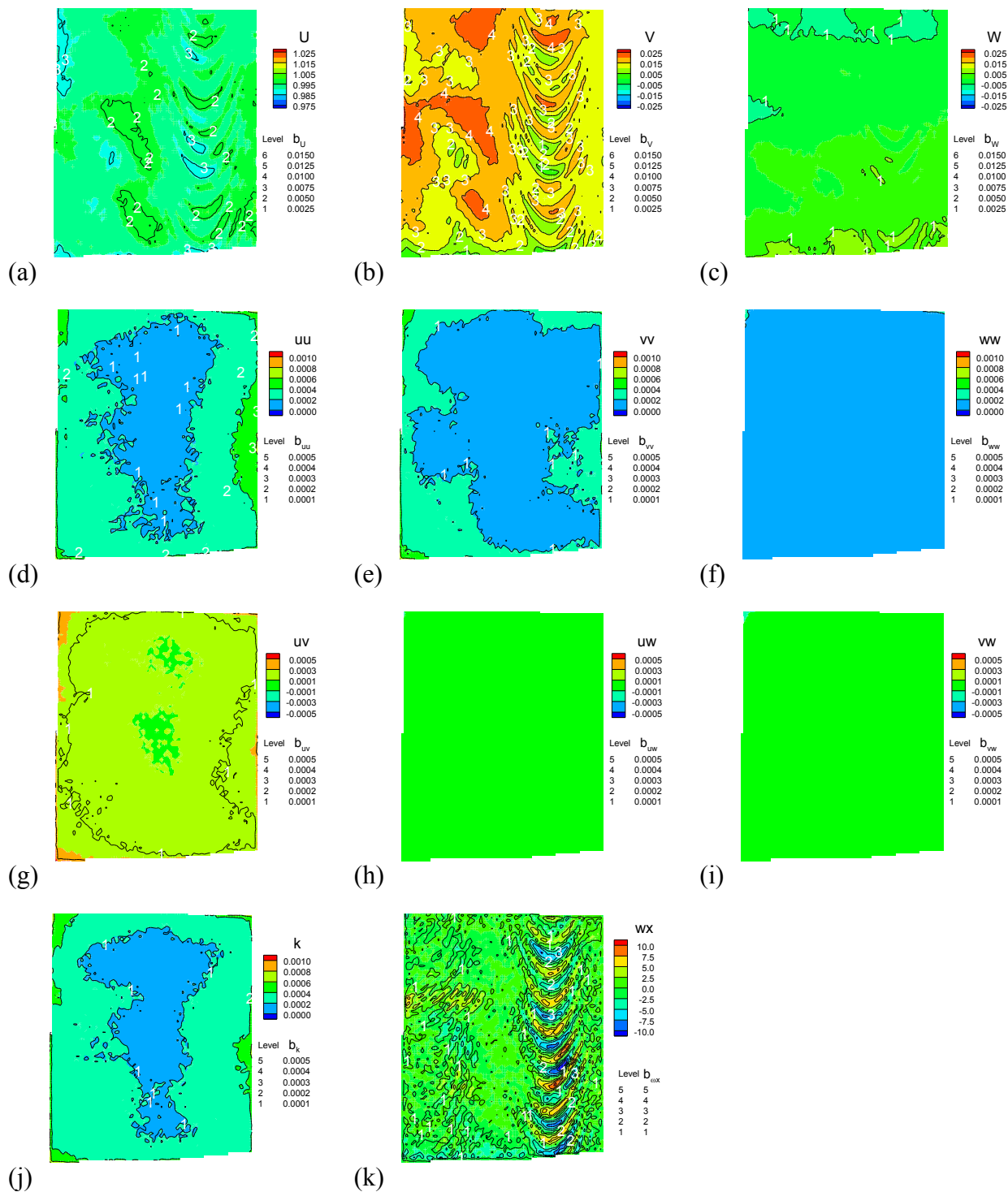
Figure 5-7 SPIV measured uniform flow field and systematic standard uncertainty for (a) *U*, (b) *V*, (c) *W*, (d) *uu*, (e) *vv*, (f) *ww*, (g) *uv*, (h) *uw*, (i) *vw*, (j) *k*, and (k) ω_x, respectively.
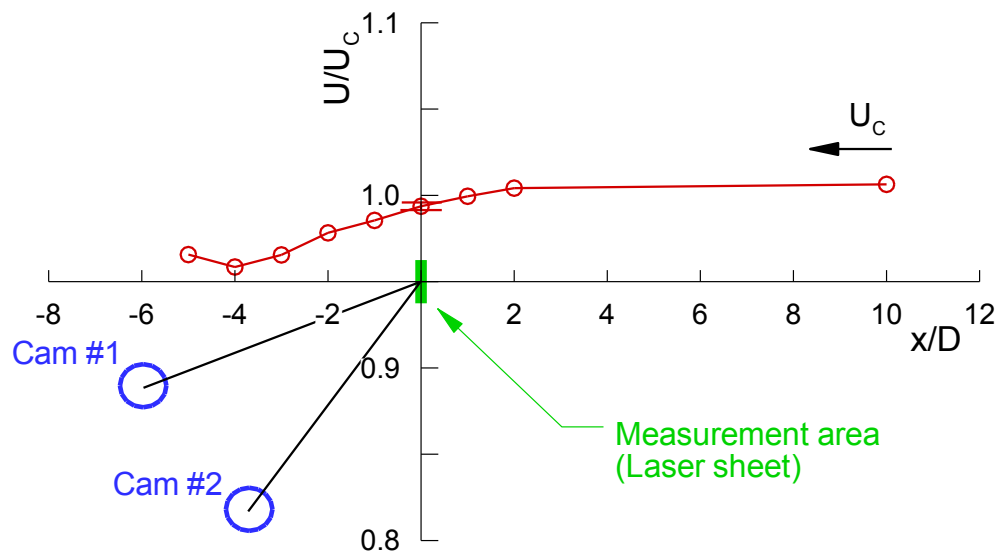
Figure 5-8 Pitot probe open water velocity U with normalized with the carriage speed U_C at various longitudinal locations, x. relative to the PIV measurement area (laser sheet plane) position $x/D = 0$, where $D = 100$ mm is the cylinder diameter of the underwater PIV camera housing.
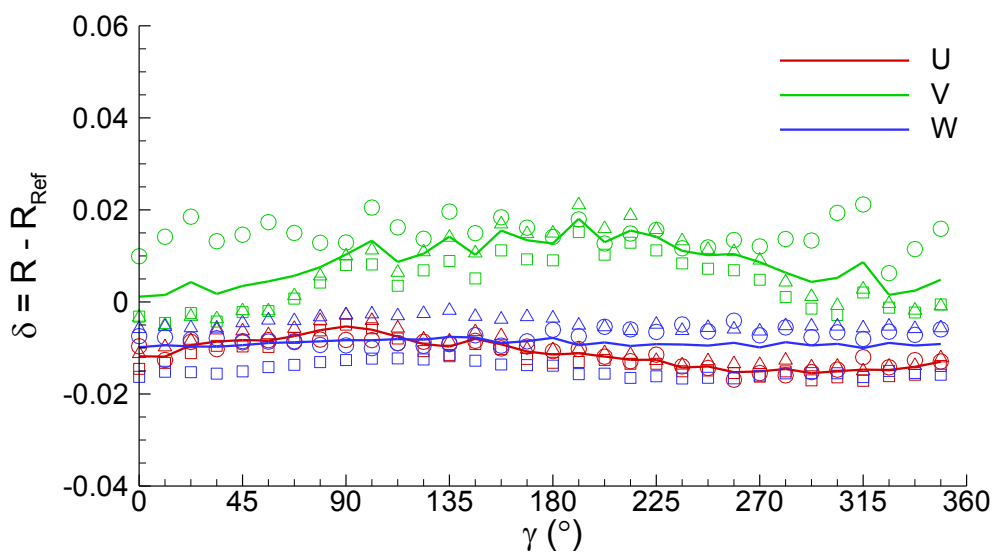

Figure 5-9 Open water pure yaw test result for SPIV UA. Symbols: □, Test 1; Δ, Test 2; ○, Test 3; and solid line is the mean δ of Test 1, 2, and 3. Each symbol shows the spatially averaged δ value over the SPIV measurement area.
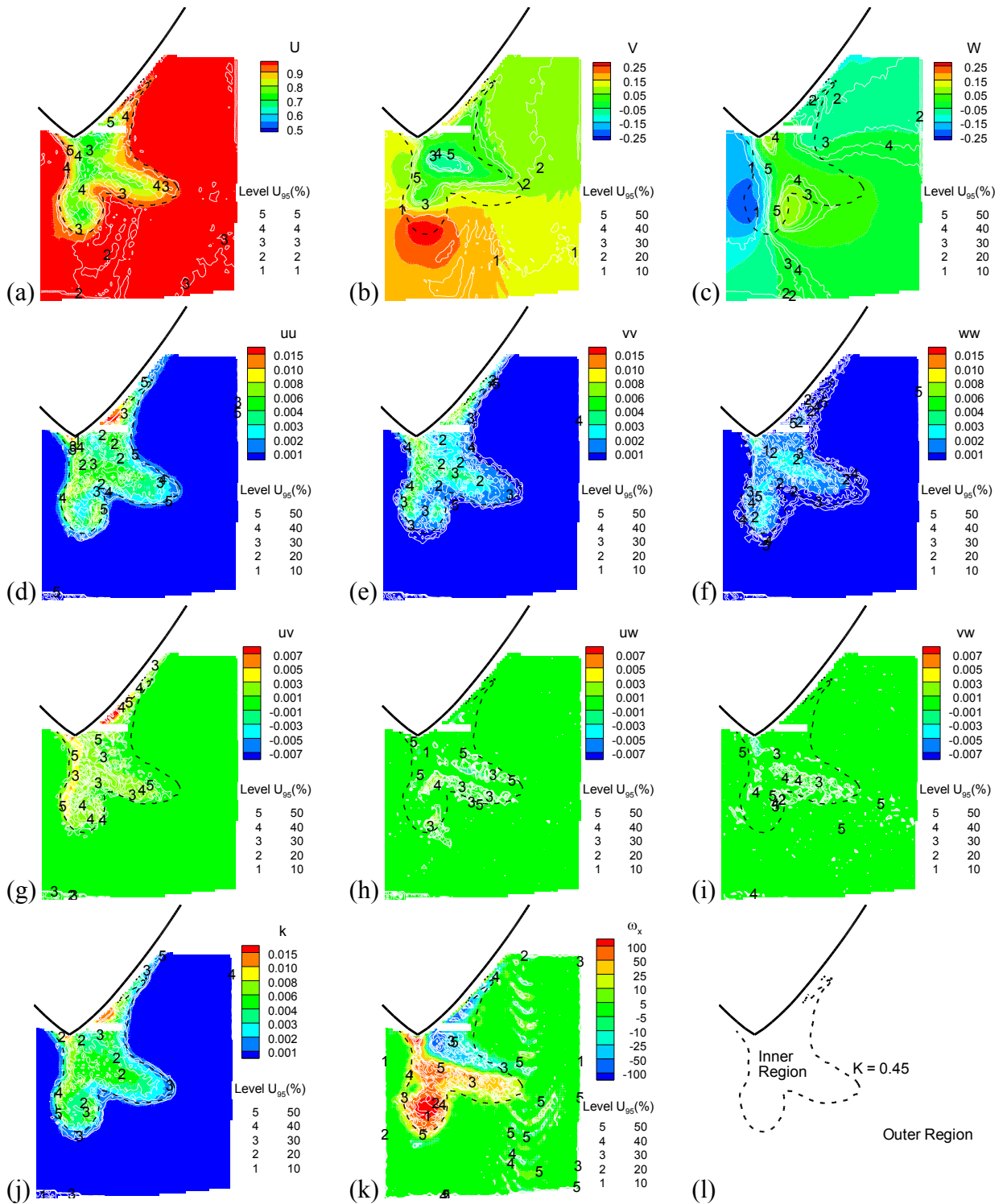
Figure 5-10 SPIV measured pure yaw flow field and relative expanded uncertainty U_{95} (%) for: (a) U, (b) V, (c) W, (d) uu, (e) vv, (f) ww, (g) uv, (h) uw, (i), vw, (j) k, and (k) ω_x, respectively. (l) Inner region, K ≤ 0.45 and Outer region, K > 0.45, where $K = \frac{1}{2}(U^2 + V^2 + W^2)$.